Techno-economic Optimization of Integrating Wind Power into Constrained Electric Networks

by

Jesse David Maddaloni
B.Eng., University of Victoria, 2005

A Thesis Submitted in Partial Fulfillment of the
Requirements for the Degree of

MASTER OF APPLIED SCIENCE

in the Department of Mechanical Engineering

© Jesse David Maddaloni, 2007
University of Victoria

All rights reserved. This thesis may not be reproduced in whole or in part, by photocopy or other means, without the permission of the author.

Techno-economic Optimization of Integrating Wind Power into Constrained Electric Networks

by

Jesse David Maddaloni
B.Eng., University of Victoria, 2005

Supervisory Committee

Dr. Andrew Rowe (Department of Mechanical Engineering)

Supervisor

Dr. G. Cornelius van Kooten (Department of Economics)

Supervisor

Dr. Peter Wild (Department of Mechanical Engineering)

Department Member

Supervisory Committee

Dr. Andrew Rowe (Department of Mechanical Engineering)

Supervisor

Dr. G. Cornelius van Kooten (Department of Economics)

Supervisor

Dr. Peter Wild (Department of Mechanical Engineering)

Department Member

ABSTRACT

Planning electricity supply is important because power demand continues to increase while there is a concomitant desire to increase reliance on renewable sources. Extant research pays particular attention to highly variable, low-carbon energy sources such as wind and small-scale hydroelectric power. Models generally employ only a simple load leveling technique, ensuring that generation meets demand in every period. The current research considers the power transmission system as well as load leveling. A network model is developed to simulate the integration of highly variable non-dispatchable power into an electrical grid that relies on traditional generation sources, while remaining within the network's operating constraints. The model minimizes a quadratic cost function over two periods of 336 hours, with periods representing low (summer) and high (winter) demand, subject to various linear constraints. The model is numerically solved using Matlab and GAMS software environments. Results indicate that the economic benefit of introducing zero cost wind into an existing system heavily depends on the existing generation mixture, with system cost reductions favoring wind penetration into thermally dominated mixtures. Results also show that integrating wind power into a generation mixture with a large percentage of coal capacity can increase emissions for moderate wind penetrations, and that coal facilities may economically replace lower cost alternatives under certain conditions.

Table of Contents

Supervisory Committee ..... **ii**
Abstract ..... **iii**
Table of Contents ..... **iv**
List of Tables ..... **vi**
List of Figures ..... **vii**
Nomenclature ..... **x**
Acknowledgements ..... **xii**
1. Introduction **1**
2. Literature Review **5**
2.1 Optimal Power Flow Models and their Solution 6
2.2 Integrating Wind into Electrical Grids 8
3. Network Model of an Electrical Grid **11**
4. Modeling Wind Generation **21**
5. The Vancouver Island Network **23**
6. Network Parameterization **30**
6.1 Network Demand 30
6.2 Generator Ramp Constraints 32
6.3 Operating Costs 32
6.4 Operating Emissions 35
6.5 Available Wind Power 36
6.6 Transmission Constraints 37
6.7 Penalty Value Associated with Power Transmission 38
7. Results and Discussion **41**
7.1 Optimal Power Flow Results 41
7.2 Wind Induced Cost on Existing Generators 47
7.3 Wind Penetration Effects on the Vancouver Island Generation Mixture, System Costs and CO_2 Emissions 49
7.4 Wind Penetration Effects on Various Generation Mixtures 53
7.4.1 System Costs and Network Export 53

7.4.2 System Emissions 62
7.4.3 Economic Dispatch between Coal and Nuclear 70
8. Discussion and Conclusions **76**
8.1 Network Constraints and Wind Induced Effects on Existing Generators 77
8.2 Operating Cost on Vancouver Island 77
8.3 Operating Cost and Network Export for Various Generation Mixtures 78
8.4 Operating Emissions for Various Generation Mixtures 79
8.5 Economic Coal Dispatching 81
8.6 Generation Mixture Attributes Leading to Beneficial Wind Integration 81
9. Recommendations **83**
Bibliography **84**
Appendix A – Calculation of Cost Parameters **88**
A.1 Calculation of Fuel Cost Coefficients for a Natural Gas Combined Cycle Facility 88
A.2 Calculation of Fuel Cost Coefficients for a Hydroelectric Facility 91
Appendix B – Cost Calculation of One Coal and One Nuclear Generator **97**

List of Tables

Table 1. Generation mixtures for various simulated regions. 27
Table 2. Ramp rate time constraints for modeled generators. 32
Table 3. Fuel and operating and maintenance cost coefficients for dispatchable generators. 33
Table 4. Carbon dioxide equivalent emission coefficients for hydrocarbon fed generators. 36
Table 5. Network connection capacities for three constraint scenarios. 38

List of Figures

Figure 1. Representation of bus i, with power leaving, moving to buses h, j and l. 13
Figure 2. The cable between buses i and j..... 13
Figure 3. The cable between buses i and j, now showing transmission loss..... 15
Figure 4. Power curve for an Enercon E70 turbine..... 22
Figure 5. The network based on the Vancouver Island grid. 24
Figure 6. The general geography of the Vancouver Island network..... 25
Figure 7. Regional capacity percentage for various generation technologies..... 29
Figure 8. The two week winter demand for each consumer bus..... 31
Figure 9. The two week summer demand for each consumer bus. 31
Figure 10. Specific cost curves over the range of generator capacity factor for the various generation technologies..... 35
Figure 11. Two week wind profile at Jordan Ridge and the associated power profile from an Enercon E70 turbine..... 37
Figure 12. Convergence of the objective function with and without the transmission penalty for various penalty values..... 40
Figure 13. The reduction of wind farm capacity factor due to transmission constraints forcing wind power truncation. 43
Figure 14. Average capacity factor as a function of increasing wind penetration for the various generators in the Vancouver Island mixture..... 45
Figure 15. Load duration curves after various amounts of wind generation for the winter demand period, unless otherwise stated. 47
Figure 16. Increase in average operating cost of all the hydro generators induced by wind intermittency..... 48
Figure 17. Vancouver Island system operating cost, with and without an amortized capital cost for the wind farm. 50
Figure 18. Vancouver Island system operating emissions for a range of wind penetrations. 52
Figure 19. System operating cost for the five simulated mixtures..... 54

Figure 20. Incremental system operating cost (compared to zero wind cost) for the five simulated mixtures. 55
Figure 21. The level and percentage of ramp constrained capacity for each mixture..... 57
Figure 22. Incremental system operating cost (compared to zero wind cost) for the five mixtures, with an amortized capital cost for the wind farm. 58
Figure 23. Peak power export from the network for the five mixtures. 60
Figure 24. Peak power export from the network due to wind excess only. 61
Figure 25. System operating emissions for the five mixtures. 63
Figure 26. Incremental system operating emissions (compared to zero wind emissions) for the five mixtures. 64
Figure 27. Average capacity factor as a function of increasing wind penetration for the various generators in the US mixture. 66
Figure 28. Generation duration curves for the coal facility (US mix) for various wind penetrations. 67
Figure 29. Carbon emissions produced by the coal facility (US mix), separated into emissions at full capacity and emissions at reduced capacity. 69
Figure 30. Average capacity factor as a function of increasing wind penetration for the various generators in the MAIN mixture. 71
Figure 31. Average capacity factor as a function of increasing wind penetration for the various generators in the NWPP mixture. 72
Figure 32. The cost of one coal and one nuclear generator meeting a 100 MW load for a single hour. 73
Figure 33. Average capacity factor as a function of increasing wind penetration for the various generators in the CAN mixture 75
Figure A1. Data points and linear trend line for the thermal efficiency of a natural gas combined cycle facility. 88
Figure A2. The original combined cycle efficiency trend and a scaled trend corresponding to current technology. 89
Figure A3. Data points showing the fuel cost of operating a natural gas combined cycle facility with respect to its part load, and a linear trend line fitted to the data points. 91

Figure A4. Data points and linear trend line for the turbine efficiency of a Francis turbine with respect to normalized water flow rate. 93
Figure A5. Data points showing the water cost of operating a hydroelectric facility with respect to its part load, and a linear trend line fitted to the data points. 96

Nomenclature

$A_{d,c}$	Slope of the linear cost function	[CAD/MWh]
$A_{d,e}$	Slope of the linear emissions function	[kg CO_2e/MWh]
$B_{d,c}$	Ordinate intercept of the linear cost function	[CAD/MWh]
$B_{d,e}$	Ordinate intercept of the linear emissions function	[kg CO_2e/MWh]
c	Cost of generation	[CAD/MWh]
$Cost$	Total cost of generation for full period T	[CAD]
$Cost_{PV}$	Total cost of generation for full period T, including the penalty cost for power transmission	[CAD]
$C_{d,c}$	Variable operating and maintenance cost	[CAD/MWh]
$Demand$	Power demand at a bus	[MW]
e	Emissions from generation	[kg CO_2e/MWh]
E	Total generation emissions for full period T	[kg CO_2e]
g	Standard acceleration of gravity	[m/s^2]
G	Power generation at a bus	[MW]
H	Height	[m]
K	Loss factor for a bus connector	[-]
L	Power loss across a bus connector	[MW]
P	Power entering or leaving a bus connector	[MW]
$\dot{Q}$	Flow rate	[m^3/s]
S	Power consumption at a bus	[MW]
$Sink$	Power sink at a bus, due to excess generation	[MW]
Δt	Time step	[hr]
β	Surface shear factor	[-]
η	Efficiency	[-]
v	Wind speed	[m/s]
ρ	Density	[kg/m^3]

Subscripts

capacity	The nameplate capacity of a generator
c	Cost coefficient
data	The location where wind data is measured
e	Emissions coefficient
Gen	The total number of generator buses
hub	The hub of a wind turbine
i, j, h, l	Bus indices
I	Incremental
k, d, n	Generator bus indices
RD,full	A value associated with a full generator ramp down
RU,full	A value associated with a full generator ramp up
t	Discrete time index
T	Total time steps
W	With wind penetration
α	Connection index
o	Without wind penetration

Acknowledgements

The author would like to thank Andrew Rowe, G. Cornelis van Kooten, Matt Schuett, Justin Blanchfield, Ned Djilali, Lawrence Pitt, Alan Tucker and Peter Wild for their contributions to this work. Funding support from the B.C. Ministry of Mines and Petroleum Resources and SSHRC Grant #410-2006-0266 is gratefully acknowledged.

1. Introduction

Global electricity demand is rapidly increasing as developed nations continue to expand and developing nations grow even faster [1, 2]. Satisfying this demand is a central issue for national decision makers and system operators. Further, while meeting the growing demand, there is increasing pressure to reduce reliance on fossil fuels, thereby reducing or slowing emissions of carbon dioxide into the atmosphere. These concerns are augmented by the need to ensure supply security.

Modeling electricity generation and consumption commonly involves a simple load leveling technique that ensures generation satisfies demand during all periods – a simple energy balance [3]. Load leveling neglects the actual transmission network that moves power from the generation sites to user locations. In practice, a utility must consider both the transmission network and load leveling, guaranteeing that demand is met and that the existing transmission system is capable of moving the power.

Optimizing the energy balance between demand and generation under various network constraints is known as an optimal power flow (OPF) solution. The objective function of the OPF problem is typically total system generation cost or total network loss [4]. The equality constraints of the problem include the bus and cable power balance equations, and the inequality constraints contain generator and transmission limitations.[1] By optimizing the OPF problem while considering non-traditional electricity generators, it is possible to shed light on the cost and emission tradeoffs that occur when these new technologies are incorporated into an established and heavily constrained network.

---

[1] A bus is defined as a conductor or assembly of conductors for collecting electric currents and distributing them to outgoing transmission cables.

The focus in this thesis is to create a network model that simulates the behavior of both highly variable (wind) and traditional generation (thermal plants, large scale hydro), while also solving the optimal power flow problem under network constraints. A direct concern is to estimate the cost and emissions of electricity generation for utilities and governments, and analyze the cost and emissions tradeoffs when installing renewable and intermittent generation capacity.

A disadvantage of low carbon energy sources such as wind and wave energy is that they can be highly variable, and the prediction of when these sources will produce specific amounts of power can be inaccurate. Electricity demand throughout a day is semi-predictable, and existing generators and networks are generally able to follow this trend easily. When large amounts of unpredictable power enter a transmission network, say from a wind farm, system operators can only rely on wind forecasting to know when they must ramp existing generators up or down to balance the remaining unmet load. The speed at which intermittent wind generation ramps up and down forces the existing generators to ramp much faster than they would in the absence of intermittent generation. Further, since prediction is not perfect, it is necessary that existing generators be on 'standby' to cover inadequate output from the intermittent source.

Due to increased ramping of existing thermal facilities, a significant decrease in operating efficiency during part load operation can occur. The decrease in efficiency corresponds to an increase in fuel consumption (on a per unit energy output basis) and thus an increase in carbon dioxide emission intensity. Therefore, the introduction of intermittent and unpredictable sources into a previously thermal dominated generation mix may not substantially reduce the net production of CO_2 within the system [5].

Analyzing these tradeoffs in emissions, as well as tradeoffs in cost and reliability, is the motive for the development of the network model.

Since this research involves the grid-integration of renewables, it is important to note the differences between dispatchable and non-dispatchable generation. *Dispatchable* electricity generation refers to facilities that are able to increase or decrease output when requested, or dispatched, to do so. This is the case for fossil-fuel power plants, nuclear plants and hydroelectric facilities with storage reservoirs. *Non-dispatchable* electricity generation refers to facilities where the power output cannot be arbitrarily controlled; the power can be curtailed to be lower than that available, but the facility cannot be dispatched to ramp up when generation is requested. Non-dispatchable facilities include run-of-river hydroelectric, wind, wave, solar, tidal and cogeneration facilities that provide space heating.

This thesis will first discuss a literature review, where existing optimal power flow formulations and wind integration research will be summarized. The network model derivation will then be provided, with a discussion of the mathematical constraints and objectives that describe the network optimization. The methods of modeling wind generation will then be discussed, including the assumed wind energy conversion device used to produce results. A description of the modeled network will follow, describing the geometry and geography of the Vancouver Island power transmission grid. The existing generation mixture will not be the only one considered, and a description of four other mixtures will then be included. The parameters used for modeling will be described next, as are the network demand, ramp rate restrictions for thermal generators, operating costs, operating emissions, the wind speed profile, transmission limitations, and the penalty

value associated with power transmission. A discussion of modeling results follows, starting with optimal power flow results for the existing Vancouver Island mixture. The effects of increasing wind penetration will be discussed using diminished load duration curves in association with generator capacity factors over the range of wind penetration. The results section will then include a discussion of how wind induces a cost on existing generators, and the difference of this cost between high and low demand periods. Wind power's effect on overall system cost and emissions will then be discussed regarding the Vancouver Island mixture, followed by a discussion regarding the overall cost and network export trends for the other four mixtures. System emission trends will then be considered for the other mixtures, particularly examining the emission trends when wind integrates with large amounts of coal fed capacity. The results section will finally examine an economic dispatch phenomenon that occurs between coal and nuclear generator types, and other types with similar cost characteristics. In the discussion and conclusions section, the key results and insights of the study are highlighted, with recommendations for future work concluding the thesis.

2. Literature Review

The work presented in this thesis is best categorized as energy system modeling. The work encompasses aspects of network modeling and the integration of new technologies into existing and constrained systems, with objectives of economic and environmental performance. Energy system modeling is a topic that is wide spread, with many research papers examining issues related to supply and demand analysis and planning, integration of new energy sources into existing systems, and the network for energy transmission and distribution in general.

Jebaraj and Iniyan's [6] review of energy system models covers energy supply and demand modeling, emission reduction models, and optimization models. The review of pertinent supply and demand models includes energy price and demand for electric utilities, electric demand for different consumer sectors of the United States, and the modeling of energy demand in general for different world regions. Emission reduction models address carbon dioxide release from current and future fossil fuel use in transportation and by utilities, as well as economic-emission linked models where the cost of mitigating carbon production is assessed. Climate models are also reviewed; these focus on the link between carbon production and global temperature rise, the link between national carbon emissions and gross national product, and the need to consider total energy use. Optimization models reviewed by Jebaraj and Iniyan included optimal configurations of generation mixtures, with and without renewable sources, which can meet demand at minimum cost, as well as optimum cost dispatch schedules for existing generation mixtures. The authors also discuss the role of renewables in models, where the allocation and type of renewable source was identified to meet regional demand under

acceptance and reliability constraints. The review of optimization models also included decentralized systems, where the capacities of small-scale renewable and thermal generators were optimized to meet local demand.

2.1 Optimal Power Flow Models and their Solution

In this thesis, optimization modeling is central. Jebaraj and Iniyan look at some optimization models, but did not include electric network optimization models, known as optimal power flow models. The optimal power flow (OPF) problem optimizes an AC electric network, where active power, reactive power and bus complex voltages are the major control variables. Bus power balances are considered for both active and reactive power, as well as cable admittance (loss), and constitute the equality constraints that are a network's power flow equations. OPF inequality constraints typically correspond to equipment ratings and recommended practices of electric transmission. The objective function of the OPF problem is typically system generation cost or system transmission loss [4]. The first nonlinear formulation of the OPF problem was provided by Carpentier [7], with alterations to the solution algorithm presented in [8-12], where the robustness and convergence speed of the optimization algorithm was enhanced. Algorithm enhancements were performed using Lagrangian multipliers on the boundary of the constraint space [8,9], with acceleration factors to enhance convergence speed [9]; researchers replaced Newton-based gradient methods with Powell and Fletcher-Powell methods [10], Hessian approximations [11], and decomposition methods [12]. An overview of nonlinear and quadratic OPF solutions is provided by Momoh et al. [4], who reviews various solution algorithms used to solve the OPF problem and their evolution

prior to 1993. The OPF formulations discussed above [8-12] typically dealt with thermal generators, with variable cost functions [4], but there is a need to consider other generation technologies within an OPF framework.

Heredia and Nabona [13] formulated the OPF problem using a mixture of thermal and hydro-electric generators, with linear power flow constraints and thermal cost as the objective function. A multi-objective OPF problem was formulated by Yalcinoz and Koksoy [14], where both generation cost and emissions were included in the objective function. The nonlinear multi-objective OPF used weight factors to create the composite objective function and the problem was solved with unmodified power flow constraints.

Lee [15] formulated the OPF problem using the location of a utility-scale fuel cell generator as a control variable. The objective was to minimize system cost subject to the network power flow equations. This formulation differed from others because the geographic placement of a system generator was used as the decision variable.

Chen [16] formulated an OPF problem with non-convex cost functions for generators, where the cost of generation could vary discontinuously, and considered market bid-price profit motives that could change generation cost non-smoothly.

A generalized OPF formulation was presented by Soderman et al. [17], who modeled electricity, heat, fuel and water flows. The problem was solved as a multiple integer linear program, minimizing the overall cost of the distributed energy system. The solution yielded the type and geometry of the whole distributed energy system under the objective of minimum cost and the constraint of given demand for various energy forms.

The foregoing research provides a description of various OPF formulations and solution methods when considering traditional generation technology, but fails to model

the behavior of both traditional and new generation technologies interacting together in an optimal way. As wind power becomes a large portion of new generating capacity, the analysis of wind penetration into existing systems must be examined.

2.2 Integrating Wind into Electrical Grids

Kennedy [3] examined the social benefit of large-scale wind power integration. The analysis considered energy, capacity and environmental costs of wind integration into a natural gas combined-cycle and coal combined-cycle dominated mixture. The energy, capacity and environmental costs served as a metric for the overall social cost (social benefit) of large-scale wind power integration. The analysis minimized the long-run average cost of operating the system under a specified reliability constraint.

DeCarolis and Keith [5] discussed the intermittency and remoteness of large-scale wind power integrated with a gas turbine combined-cycle and compressed air energy storage (CAES) system. A carbon tax was employed as a sensitivity parameter to measure how the optimal generation mixture changed with varying levels of the variable fuel price. The objective of the model was to minimize average electricity cost by arranging capacities of wind arrays, transmission cables, a storage system and back up gas turbines geographically within a simple network. The simple network encompassed a single demand fed by various generating sources and with varying transmission capacities.

Greenblatt et al. [18] discussed the base load generating potential and economic viability of wind-CAES systems competing with wind-thermal systems. A simple one-cable generation and transmission system was modeled, where wind and CAES fed a

single transmission cable, and thermal generators were located at the single demand node to satisfy unmet demand. The objective was to minimize the total levelized cost of energy by changing the capacities of the wind farm, the CAES system, and the thermal plants, and the voltage of the transmission cable. Fuel price was then altered using a variable carbon tax to examine various optimal system configurations.

Denholm and Kulcinski [19] assessed the technical and environmental performance of several wind-CAES systems that could be operated in the United States Midwest to provide base load generation. The objective in this analysis was to maximize constrained transmission capacity (maximize the system capacity factor) in order to provide a consistent amount of base load, with the size of the wind farm considered to be the major control variable and the capacity of the CAES system as an input parameter.

A study presenting a wind-pumped hydro system capable of feeding electric demand on the Aegean islands was developed by Kaldellis and Kavadias [20]. A wind farm in conjunction with a pumped hydro facility was analyzed, with excess wind power feeding a desalination plant. The objective of the analysis was to obtain local electricity supply independence on the islands; this was done by minimizing the consumption of delivered oil under the constraint of a feasible start-up cost. The variables considered were the wind farm capacity, the geometry of the water reservoirs, the size and types of pumps and turbines, the operation plan of the existing thermal generators, and the size of the desalination plant.

Elhadidy and Shaahid [21] analyzed a decentralized wind-diesel-battery system that provided an electric source for a commercial/residential building in a hot climate.

The size and type of wind generators, the battery capacity and the operational hours of the diesel generator were variable in the analysis.

Weisser and Garcia [22] examined an isolated diesel-fed electric network by restricting the integration of wind power into that network. The model was used to discuss supply reliability and power quality at increasingly high levels of wind penetration into medium-sized, diesel-fed grids. The authors considered a short time step measured in seconds, and the medium scale of minutes to determine how the existing system would buffer wind intermittency and its ability to maintain power quality.

The wind integration research describes wind penetrating into various systems, with some consideration of simple transmission limitations. There exists a need to consider both the load leveling of highly intermittent wind power into the existing and constrained system, as well as the optimal solution of the OPF through the transmission network. Including existing generator ramp rate constraints enables one to model the ability of existing generation to balance the variance introduced by the wind source, while the inclusion of variable costs and emissions from the existing generators addresses the altered economic and environmental performance of the technology due to the introduction of wind. Solving the OPF problem while considering the mixture of wind and existing generator technologies will then ensure that the existing network can transmit the power to the demand location, and that power is dispatched in the most economic way. This analysis is provided in this thesis.

3. Network Model of an Electrical Grid

The network model consists of an objective function that is to be minimized subject to a set of equality and inequality constraints. The objective function is formulated to be total network cost. The equality constraints consist of bus power balance equations for each bus, and the cable power balance equations for each cable. The inequality constraints consist of generator capacity limits, cable power limits, export limits, and ramp rate limits.

The major operational assumptions of the current network model are as follows:

1. Electricity production must always satisfy demand.
2. At any instant in time, a bus connection must be unidirectional; power can only flow in one direction across a cable. Bidirectional flow across a connection is possible, just not simultaneously.
3. Dispatchable generation is constrained by the ramp rate.
4. Non-dispatchable generation is considered 'must run', but truncation is allowed under certain circumstances of excess generation.
5. The power along each cable is constrained unless otherwise stated.
6. Cost of generation varies linearly as a function of capacity factor.
7. Emissions vary linearly as a function of capacity factor.

The model assumes a DC formulation of electricity production, transmission and consumption, omitting reactive and active power elements and simply dealing with absolute power. An AC formulation is not considered because this study is not aimed at examining network stability or power quality, which exists at the timescale of grid frequency (less than one second). Although the time resolution of the model is hourly, the

timescale with respect to energy policy is much longer, looking at system planning for future low cost generation mixtures. AC modeling analyzes the effects of generators on a very short timescale, but the AC analysis is not required for the motives of this thesis, and a DC analysis allows simplification of the network model such that other interactions can be analyzed at more depth. The model optimization assumes the role of the system operator, aiming to minimize the cost of the entire system; this occurs instead of analyzing the cost of individual generators competing in a power pool bidding system. This means that the solution may raise the cost of an individual generator if it means a lower overall cost. The model also assumes that the cost for generators varies linearly with capacity factor, while in reality these trends are non-linear. Linearization of generation cost is performed to simplify the model and allow an optimal solution to be obtained over a longer time period.

The network model is composed of geographically arranged buses, with each bus connected to various other buses using links. Each bus represents a transmission network substation, and the bus linkages represent the transmission cables between each station. Each bus may have its own local generation or demand, while also allowing power to pass through it en route to other consuming buses. These assumptions in conjunction with the convention shown in Figure 1 lead to the bus power balance equation:

$$\sum_{j}^{links} P_{i,j,t} + S_{i,t} + Sink_{i,t} - G_{i,t} = 0 \quad \forall \quad i = 1,2,...,buses \;\; \& \;\; t = 1,2,...,T \,, \qquad (1)$$

where S denotes power consumption, *Sink* refers to power export or storage, and G denotes power generation. Equation (1) constitutes a separate constraint for each bus i, and holds for every time period t. The bus power balance equation accounts for load

leveling and transmission, and ensures that demand is met at each bus for each time. The summation term accounts for all connections between buses j ($j=1,2,\ldots,cables$) and bus i. The power moving from a bus across a cable is defined positive leaving the bus as indicated by Figure 1, where a visual representation of this convention is employed.

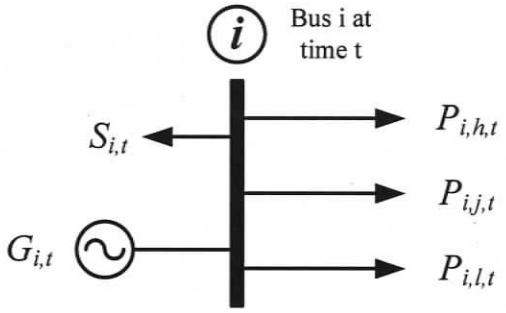

Figure 1. Representation of bus i, with power leaving, moving to buses h, j and l.

The $P_{i,j,t}$ term in Figure 1 shows the power leaving bus i for bus j at time t. The connection between buses i and j at time t is considered in Figure 2. Since power is defined as positive when leaving a bus, Figure 2 shows the two terms $P_{i,j,t}$ and $P_{j,i,t}$ entering the cable from different directions. The unidirectional constraint on the cable specifies that one of the $P_{i,j,t}$ or $P_{j,i,t}$ terms must always be positive, while the other must always be negative.

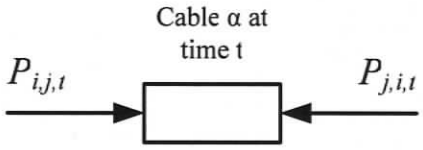

Figure 2. The cable between buses i and j.

The directional convention in Figure 2 leads to the cable power balance equation:

$$P_{i,j,t} = -P_{j,i,t} \qquad (2)$$

Equation (2) does not account for power loss across a transmission cable. This is neglected to simplify the network and allow the optimization problem to be formulated with linear constraints. The simultaneous solution of Equations (1) and (2) ensures that power generation will always be sufficient to meet demand ($\sum_{i}^{nodes} S_i$) in each time period.

Power loss across a cable can be considered by re-writing Equation (2) as $P_{i,j,t} + P_{j,i,t} = L_{\alpha,t}$, where $L_{\alpha,t}$ is the power loss across cable α at time t. An additional non-linear constraint must be incorporated to take account of the transmission loss, which could be calculated by multiplying the maximum power entering the cable by a constant loss factor K: $L_{\alpha,t} = \max\{P_{i,j,t}, P_{j,i,t}\} \cdot K_{\alpha}$. The directional cable balance convention is provided again in Figure 3, this time showing the loss leaving the cable. To calculate loss using this approach, the loss factor K must be multiplied by the power term entering the cable (or the maximum or positive power term) to ensure that power is reduced along the direction of transmittal. If the loss was calculated using the minimum or negative power term then power would increase along the direction of transmittal, and power would be gained from transmission and not lost. Including a discontinuous 'max' operator as a network constraint adds to the complexity of finding an optimum solution, and, for some solvers (discussed below), this requires too short a time period for which it is possible to obtain feasible solutions. The discontinuous loss constraint was not included in the current formulation in order to make the constraint set purely linear and allow an optimal solution to be found over longer time periods.

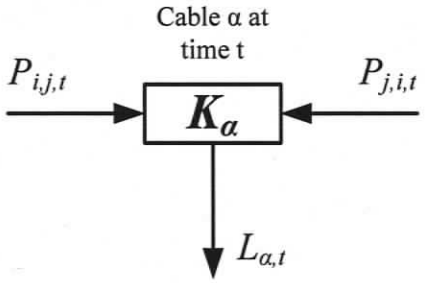

Figure 3. The cable between buses i and j, now showing transmission loss.

The power moving across each cable, both positive and negative, must be constrained so that transmitted power does not exceed the cable capacity. The cable capacity constraints are written as follows:

$$P_{i,j,t} \leq P_{\alpha,\max} \quad \forall t = 1,...,T \tag{3}$$

$$P_{i,j,t} \geq -P_{\alpha,\max} \quad \forall t = 1,...,T \tag{4}$$

where T is the number of time steps (hours, minutes, seconds) to be analyzed in the model.

For dispatchable generating sources, power generation is limited to the maximum output available from a facility:

$$G_{d,t} \leq G_{d,capacity} \quad \forall\, d = 1, \ldots, \text{dispatchable generators}; t = 1, \ldots, T. \tag{5}$$

Dispatchable generation facilities are also ramp-rate constrained, so that the increase or decrease in power output over a single time step is limited to be within the operating ability of the facility. The respective ramp-up and ramp-down constraints are:

$$\frac{G_{d,t} - G_{d,(t-1)}}{\Delta t} \leq \frac{G_{d,capacity}}{\Delta t_{RU,full}} \forall\, d = 1, \ldots, \text{dispatchable generators}; t = 2, \ldots, T. \tag{6}$$

$$\frac{G_{d,t} - G_{d,(t-1)}}{\Delta t} \geq -\frac{G_{d,capacity}}{\Delta t_{RD,full}} \forall\, d = 1, \ldots, \text{dispatchable generators}; t = 2, \ldots, T. \quad (7)$$

where the terms $\Delta t_{RU,full}$ and $\Delta t_{RD,full}$ denote the time required for a facility to ramp up from zero to full capacity and the time to ramp down from full capacity to zero, respectively. The numerators on the left hand sides of Equations (6) and (7) are the changes in power output that occur during a time step. The right hand sides of (6) and (7) are the limits by which a facility can either increase or decrease output over a single time step. Non-dispatchable generation is not ramp-rate constrained, but is considered *must run*. This constrains the network so that any power available from a non-dispatchable source must be used by the network during that time period:

$$G_{n,t} = G_{n,t,available} \;\forall\, n = 1, \ldots, \text{non-dispatchable generators}; t = 1, \ldots, T. \quad (8)$$

Finally, generation from all facilities, dispatchable or non-dispatchable, can never be negative:

$$G_{k,t} \geq 0 \;\forall\, k = 1, \ldots, \text{generators}; t = 1, \ldots, T. \quad (9)$$

The power consumption at a typical bus will simply follow the consumer demand at that bus (substation) for the given time period t. It is assumed that demand at each bus is known *a priori*. The nodal consumption constraint is thus

$$S_{i,t} = Demand_{i,t} \;\forall\, i = 1, \ldots, \text{buses}; t = 1, \ldots, T. \quad (10)$$

Due to the *must run* constraint (8) and the ramp-down constraint (7), there may exist some time periods when generation is forced to exceed demand. If there is no sink to absorb this excess, the model will not find a feasible solution. This requires one or more buses to have the potential to either consume power for storage or export power to a location outside the network. Both options take the form of added (sink) constraints:

$$Sink_{i,t} \geq 0 \forall i,t \tag{11}$$

$$Sink_{i,t} \leq Sink_{capacity} \forall i,t\,, \tag{12}$$

where a bus may have a sink term that is able to increase in the event of excess generation. The amount of excess power that can be absorbed is limited by the rate of storage in Equation (12), but not with respect to the maximum amount of energy stored over the full time period T, which is given by $\sum_{t}^{T}\left(Sink_{i,t} \cdot \Delta t\right)$. Future research will focus on the inclusion of such an energy constraint, as well as the round-trip storage efficiencies when using this energy to satisfy demand at some future time. If excess generation occurs during a time step, dispatchable generators may be able to absorb the excess by loading the network, instead of absorption occurring at an additional sink. The possibility of loading the network with a negative generation term has not been considered.

The objective is to minimize the cost of generation over the entire period T:

$$Cost = \sum_{t}^{T}\sum_{k}^{Gen} c_{k,t} \cdot G_{k,t} \tag{13}$$

In (13), the cost coefficients (c) are a function of the level of generation (G) for dispatchable generators, but are constant for non-dispatchable generators. For dispatchable generation, the cost coefficients are assumed to follow a linear trend with respect to the part-load operation of the facility:

$$c_{d,t} = A_{d,c} \cdot \left(\frac{G_{d,t}}{G_{d,capacity}}\right) + B_{d,c} + C_{d,c}\,, \tag{14}$$

where the fraction $G_{d,,t}/G_{d,capacity}$ represents the normalized part-load operation of (dispatchable) generator d. The slope $A_{d,c}$ and the ordinate intercept $B_{d,c}$ of the linear

approximation can be determined using the efficiency of a generator during part-load operation, and the cost per unit input energy into the facility. The $A_{d,c}$ and $B_{d,c}$ cost coefficients account for fuel costs only, with the $C_{d,c}$ term accounting for variable operating and maintenance (O&M) costs. Actual values for $A_{d,c}$, $B_{d,c}$ and $C_{d,c}$ are discussed in the network parameterization section (Section 6). The slope term is typically negative, resulting in an increased cost per unit output when operating below the full capacity of the generator.

The objective function (13) only considers dispatchable generation cost, and a penalty contribution must be included in the objective function to include a cost of power transmission. If transmission loss was considered in the model formulation, then a penalty would already be assigned to power transmission; with increased transmission leading to increased loss, which in turn leads to increased generation and system cost. Due to the elimination of the loss equations, a penalty for power transmission must be included in the objective function.

Including this penalty will also eliminate the possibility of un-generated power traveling around a loop of buses within a considered network. The network balance equations (1) and (2) are formulated such that a loop of buses could allow extraneous power to be routed around the loop. The looped power would increase the power at a bus when entering and remove the same amount of power when leaving, thus still satisfying the bus balance equation. If a penalty function is applied to the transmitted power along each connection, then the objective would minimize cost as well as eliminate any unnecessary power looping throughout the network. The objective now includes dispatchable generation cost and a cost associated with power transmission:

$$Cost_{PV} = \sum_{t}^{T}\sum_{k}^{Gen} c_{k,t} \cdot G_{k,t} + PV \cdot \sum_{t}^{T}\sum_{\alpha}^{Links} P_{\alpha,t}^{2} \tag{15}$$

The objective function in (15) will still approximate dispatchable generation cost if the penalty for power transmission is small enough to make the penalty contribution to the objective negligible. Each bus connector α has two power terms associated with it (for example: $P_{i,j,t}$ and $P_{j,i,t}$), but only one term needs to be considered for the penalty function. If one of the power terms associated with connection α is then squared (P_{α}^{2}), then it will guarantee that the power transmission term will be positive, irrespective of which direction power is flowing across the cable. One power term for each connection and each time period is squared and summed for all connections and all time periods, then multiplied by the penalty value (PV), and added to the cost portion of the objective function. The objective (15) will now minimize dispatchable generation cost while eliminating excess power traveling around bus loops.

Total system emissions are also calculated over the full time period T:

$$E = \sum_{t}^{T}\sum_{k}^{Gen} e_{k,t} \cdot G_{k,t} \tag{16}$$

In (16), the emissions coefficients (e) are a function of the level of generation (G) and are again assumed to follow a linear trend with respect to the part-load operation of the facility:

$$e_{d,t} = A_{d,e} \cdot \left(\frac{G_{d,t}}{G_{d,capacity}} \right) + B_{d,e}, \tag{17}$$

The slope $A_{d,e}$ and the ordinate intercept $B_{d,e}$ of the linear approximation are determined using the efficiency of a generator during part-load operation, and the equivalent carbon dioxide emissions per unit input energy into the facility. The slope term is again typically

negative, resulting in increased emissions per unit output when operating below the full capacity of the generator.

Optimization of objective (15) subject to constraints (1) through (12) and (14) is performed using GAMS [23]. The problem is a discrete dynamic quadratic program with linear constraints, and is solved using the MINOS and CPLEX solvers. In the current application, GAMS solves the optimal control model over a period of two weeks at an hourly resolution (although any length of time and time step could be chosen), and Matlab is used to feed parameters to the GAMS routine for each hour. Matlab is the main shell for the network model and is used to loop the GAMS optimization as well as perform general data management. Data such as nodal demand and wind speeds are input into Matlab, the m-file then calls GAMS for each optimization and returns the solution.

Due to the discrete dynamic operation of the model, starting values are required for each optimization period so that state equations (6) and (7) may be initially defined. For the first optimization period, the starting activities are set as the optimal static solution of the first time period. For subsequent optimization periods, the starting activities are the final activities from the previous optimization period.

4. Modeling Wind Generation

All results assume that wind speeds are perfectly predicted over the total period T of the optimal solution, with wind profiles derived from wind measurements at actual locations. Simulations also assume that all turbines experience the same wind speed at the same time, neglecting spatial dispersion of generation across the area of the turbine farm, if multiple turbines are to be considered.

To approximate generated wind power given wind speed, the measured wind speed is first scaled to approximate wind speed at the hub height of the wind turbine; then a manufacturer's power curve is used to interpolate a generation level given hub wind speed. The scaling of wind speed from measured height to turbine hub height is performed using an exponential scaling equation [24]:

$$v_{hub} = \left(\frac{H_{hub}}{H_{data}} \right)^{\beta} \cdot v_{data} \tag{18}$$

The terms v_{hub} and v_{data} in (18) represent the wind speed at the hub height (H_{hub}) and data measurement height (H_{data}), respectively. In (18), β is the surface shear factor and depends on the ground cover at the turbine location. For all results, the shear factor was chosen to be 0.14, the mean value between short grasses and low vegetation [25].

The turbine power curve used for all results approximates power generation from an Enercon E70 turbine [26], and is shown graphically in Figure 4. The Enercon E70 turbine has a rated capacity of 2050 kW, a cut-in wind speed of 2.5 m/s, and cut-off wind speed of 31 m/s. When hub wind speed drops below the cut-in speed, or rises above the cut-off speed, the generation from the turbine is modeled as zero. If the hub wind speed is

between the cut-in and cut-off speeds, then the turbine generation level is linearly interpolated between the points on the power curve.

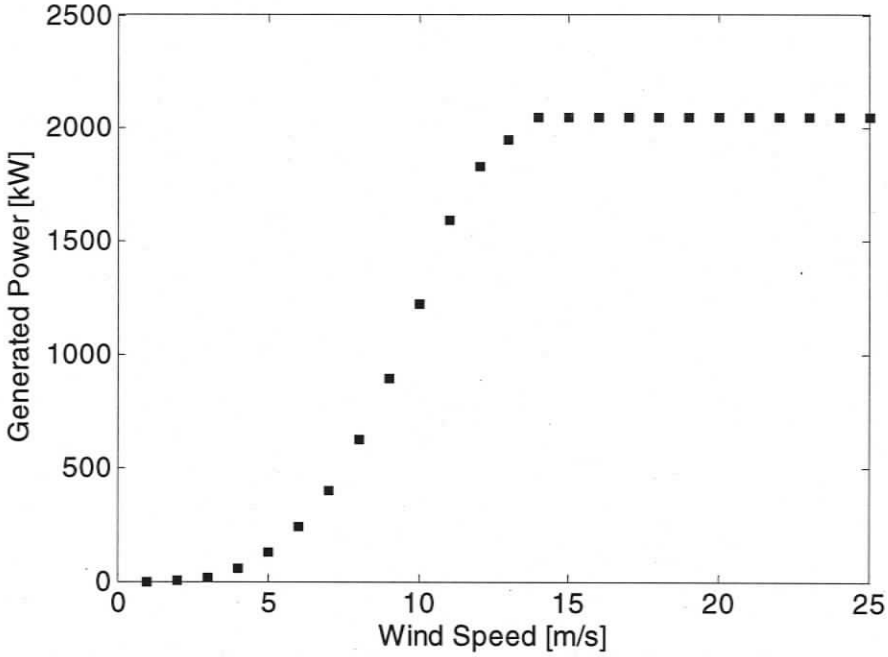

Figure 4. Power curve for an Enercon E70 turbine.

5. The Vancouver Island Network

A small network is used to validate the constrained operation of the model and to provide insights regarding wind penetration into different generation mixtures. As shown in Figure 5, the test grid is composed of 7 buses (labeled 1 through 7) and 9 cables (labeled *a* through *i*). The algebraic terms for power moving out from each bus are indicated in Figure 5, neglecting transmission loss. The network is formulated to represent a simplified version of the existing network on Vancouver Island, a 500 km long island off the west coast of British Columbia, Canada. The simplified network is shown overtop a geographic image of Vancouver Island in Figure 6.

Buses 1, 2, 3, 5, 6 and 7 make up the Vancouver Island network, and bus 4 is a B.C. mainland bus connected to the Island network via cable *d*. Cable *d* is modeled as a high voltage submarine cable with the capacity to transmit either to or from the Island. The required export/storage sink, described by Equations (11) and (12), is placed at bus 4 so that any excess generation can be exported to the B.C. mainland. Power is consumed at buses 1, 2, 3, 5, 6 and 7 and the mainland bus 4 consumes power for export only.

Buses 1, 2, 3, 4 and 7 all generate power. The existing Vancouver Island generation mixture has thermal generators located at buses 1 and 4 and large-scale hydroelectric generators are located at buses 1, 3, 4 and 7; this mixture is labeled in Figure 5. The wind farm generator is located at bus 2, and will remain there for all simulations.

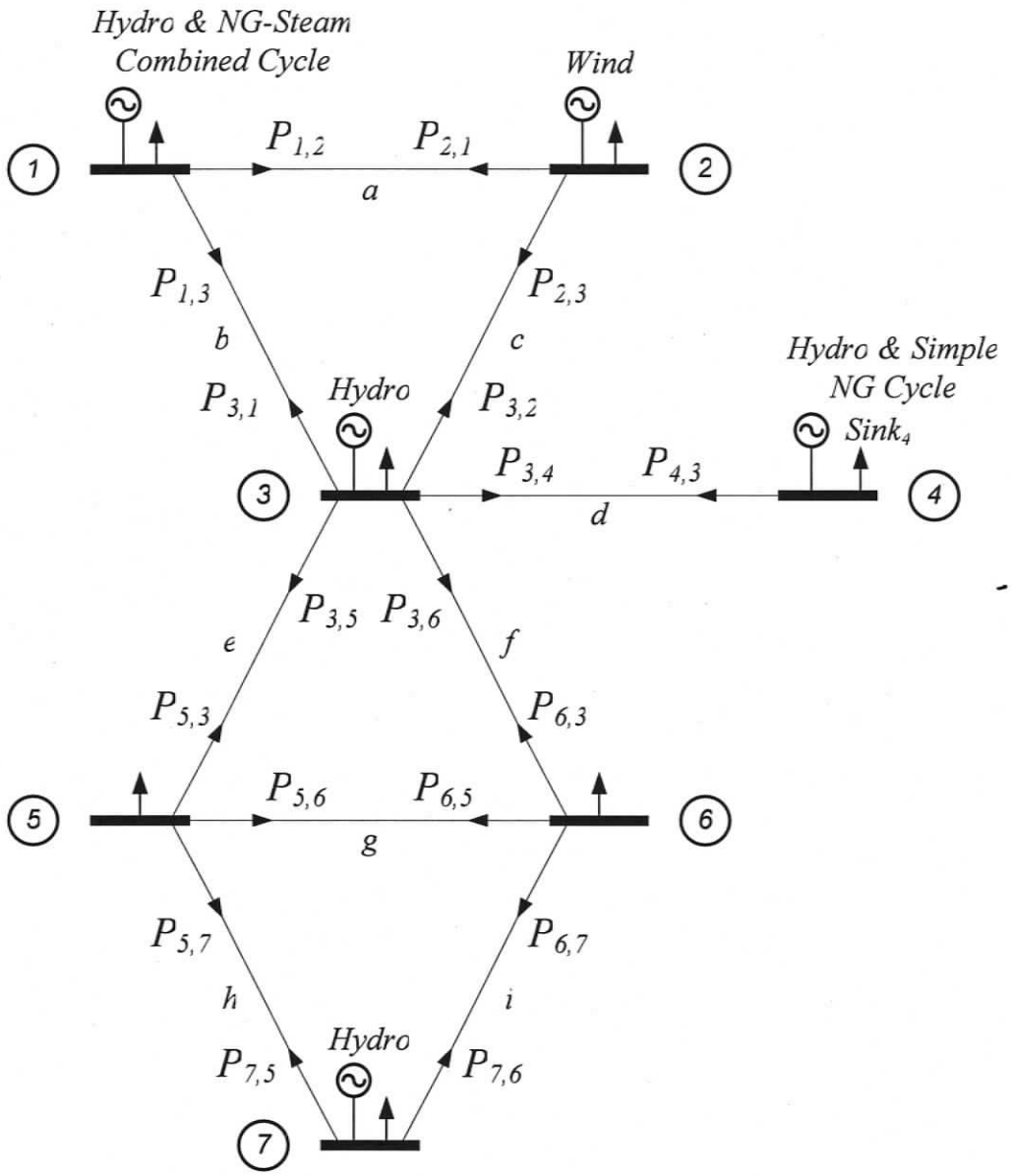

Figure 5. The network based on the Vancouver Island grid.

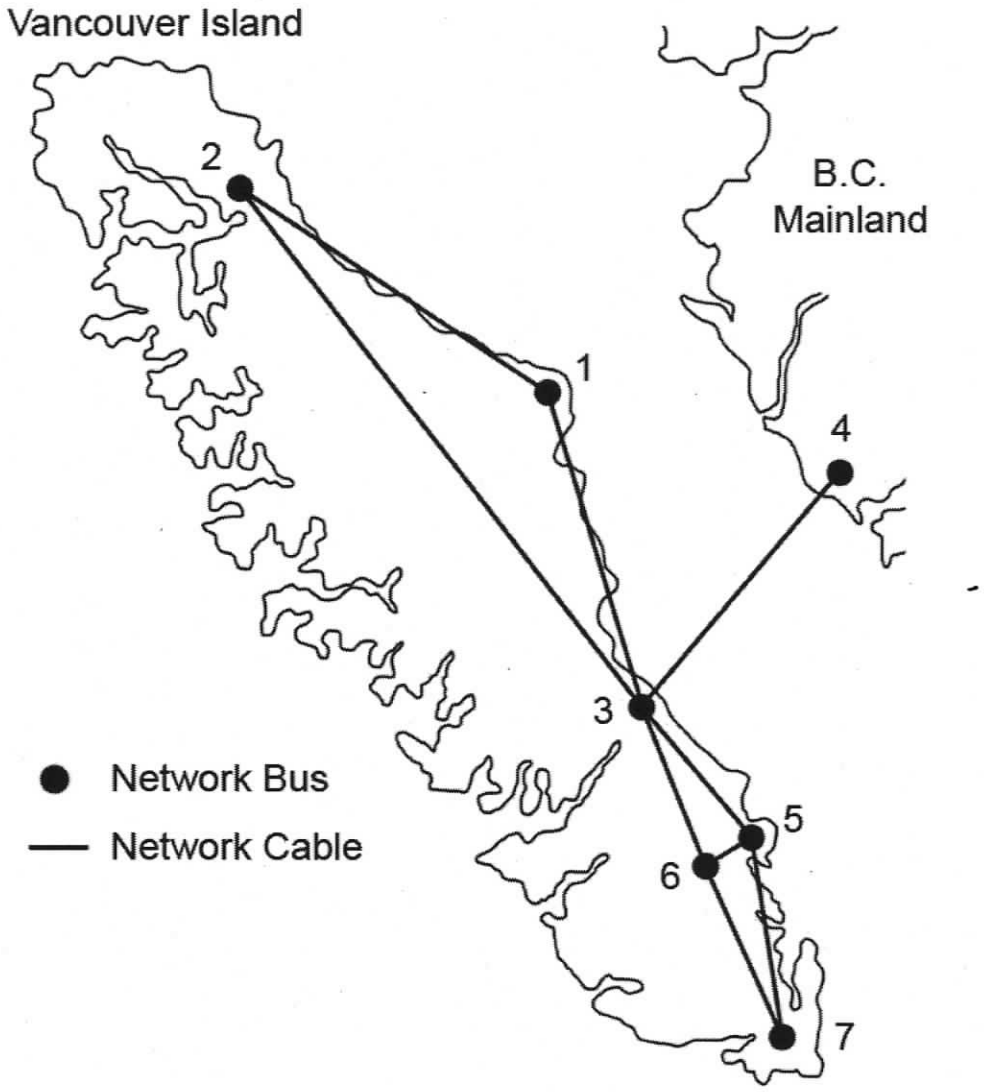

Figure 6. The general geography of the Vancouver Island network.

The thermal generator at node 1 is a combined-cycle, natural gas-steam unit with a capacity of 290 MW. The thermal generator at bus 4 is a simple cycle natural gas unit, with a capacity of 400 MW. The hydroelectric generators at buses 1, 3, 4 and 7 have capacities of 237, 57, 900 and 170 MW, respectively. The generator types and capacities have all been chosen to represent the actual generation capability on Vancouver Island.

The generation technologies located at each node will not remain static for all results, and will differ for simulations that consider generation mixtures other than what currently exists on Vancouver Island. For this purpose, we employ generation mixtures representative of the Canada aggregate generating mix, as well as those of the US Northwest, US Mid-America Interconnected Network, and the US aggregate power system. This provides an excellent way to examine the effects of wind power on systems with substantially different reliance on energy sources.

The generation mixture for Vancouver Island and other related or relevant regions are provided in Table 1, as are the generation technologies, bus locations, and capacities of the various generators. It can be seen in Table 1 that the generating capacity at each node is altered from the actual Vancouver Island capacity breakdown, this is performed to better approximate the actual technology percentages in each region.

Table 1. Generation mixtures for various simulated regions.

Generation Technology	Bus	Capacity [MW]
Existing Vancouver Island (VI)		
Hydro	1	237
NG CC [1,2]	1	290
Hydro	3	57
Hydro	4	900
NG SC [3]	4	400
Hydro	7	170
TOTAL		**2054**
Canada Aggregate (CAN)		
Nuclear	1	255
Hydro	1	300
Petroleum CC	3	70
Hydro	4	900
IGCC [4]	4	398
NG CC	7	131
TOTAL		**2054**
United States Aggregate (US)		
Nuclear	1	238
Hydro	1	145
P CC [5]	3	73
IGCC	4	1032
NG CC	4	396
Nuclear	7	170
TOTAL		**2054**
United States Northwest Power Pool (NWPP)		
IGCC	1	249
NG CC	1	331
P CC	3	20
Hydro	4	885
NG CC	4	457
Nuclear	7	112
TOTAL		**2054**

Table 1. Continued

Generation Technology	Bus	Capacity [MW]
United States Mid-America Interconnected Network (MAIN)		
NG CC	1	232
NG CC	1	284
Hydro	3	29
IGCC	4	1044
Nuclear	4	363
P CC	7	101
TOTAL		**2054**

[1] NG is an abbreviation for natural gas.

[2] CC is an abbreviation for combined cycle. The combined cycle technologies discussed in this paper refer to hydrocarbon-steam combined cycles.

[3] SC is an abbreviation for simple cycle, which refers to hydrocarbon combustion through a gas turbine.

[4] IGCC is an abbreviation for integrated coal-gasification combined cycle, which also uses steam.

[5] P is an abbreviation for petroleum, a hydrocarbon fuel.

The generation mixture for Vancouver Island was obtained from BC Hydro [27], and the Canada aggregate mixture was obtained from the Canadian Electricity Association [28]. The United States aggregate mixture was obtained from the Energy Information Administration [29], as were the mixtures for both the Northwest Power Pool and the Mid-America Interconnected Network [30]. The existing renewable capacity located in each simulated region, other than hydroelectric, has been neglected due its almost negligible contribution to the power mix. The natural gas and petroleum fed generation for regions other than Vancouver Island have been assumed to use combined cycle technology only. The percentage breakdown of energy source for each simulated region is shown graphically in Figure 7.

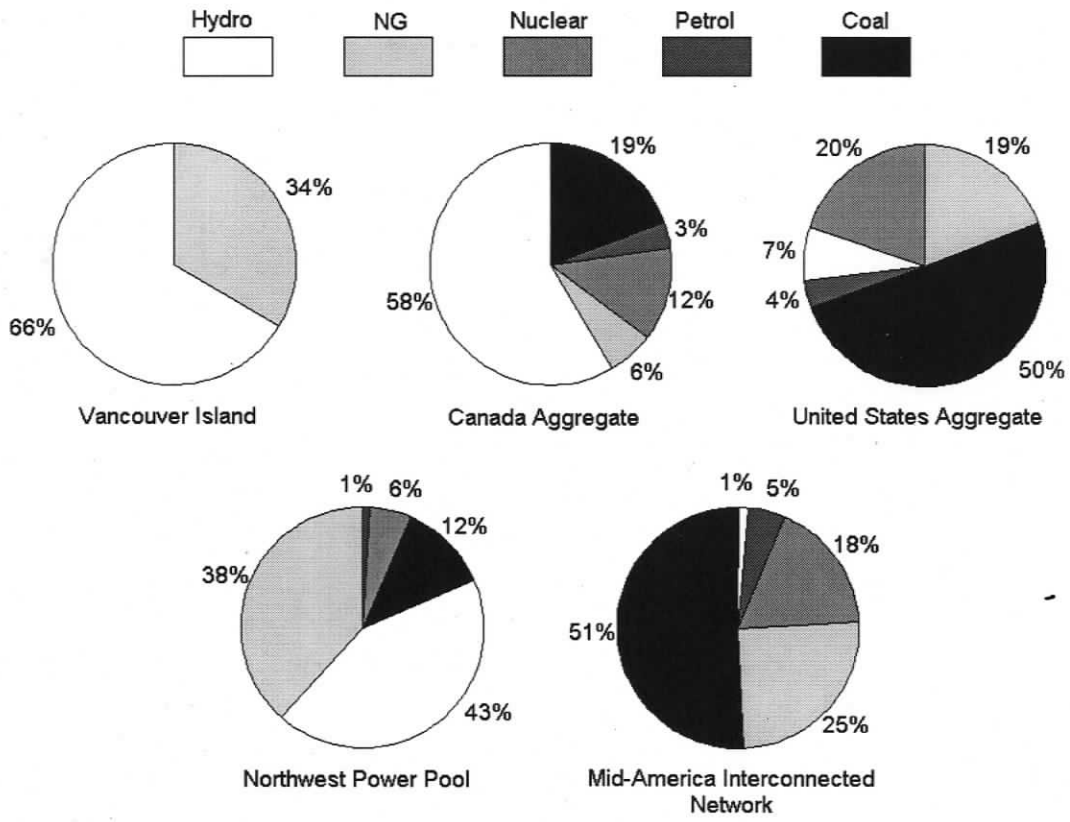

Figure 7. Regional capacity percentage for various generation technologies.

6. Network Parameterization

All solutions employ 336 periods, each representing one hour over two weeks, with the optimization assuming rational expectations – demand is known and non-dispatchable power is perfectly predicted. Solution variables for this optimal power flow problem include for each hour, all 18 of the cable power terms ($P_{i,j}$), the six levels of power generation from the six dispatchable generators, and the export/storage sunk power at bus 4.

6.1 Network Demand

Demand data for Vancouver Island were provided by BC Hydro [27] in the form of a conglomerated hourly load for the entire Island for 2003. Two 336 hour demand profiles are used to demonstrate the network operation over both high (*winter*) and low (*summer*) demand periods. The high demand profile is the actual Vancouver Island demand for December 18-31, 2003, while the low demand profile is the actual demand for July 9-22, 2003. The winter and summer demand profiles are shown in Figures 8 and 9, respectively, and have respective energy demands of 508 GWh and 366 GWh.

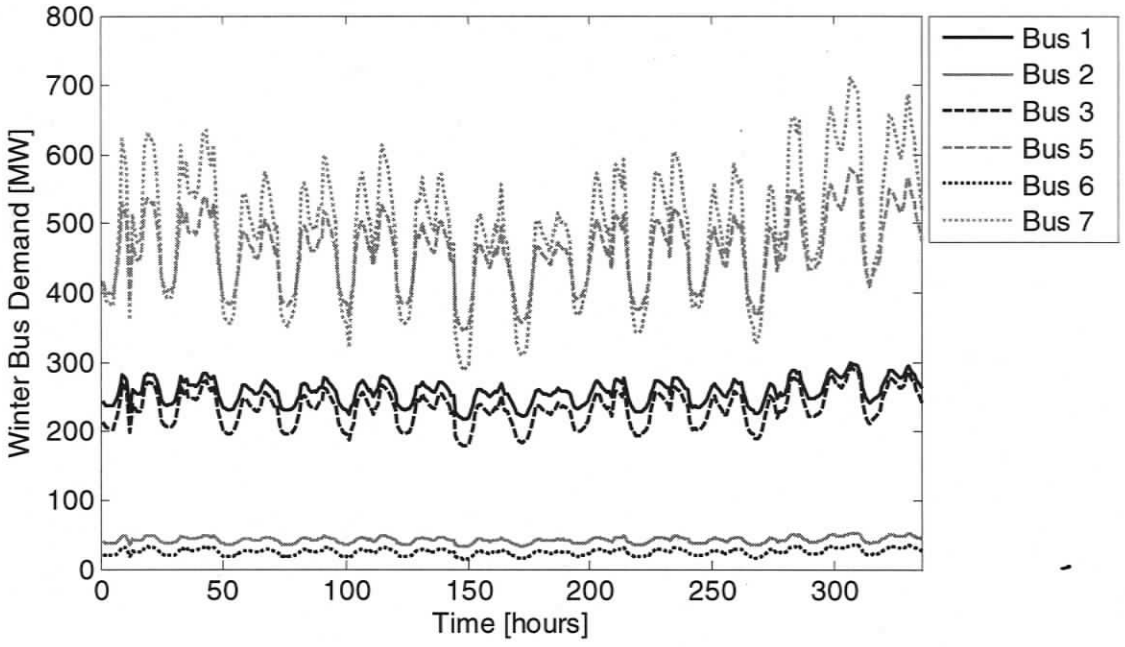

Figure 8. The two week winter demand for each consumer bus.

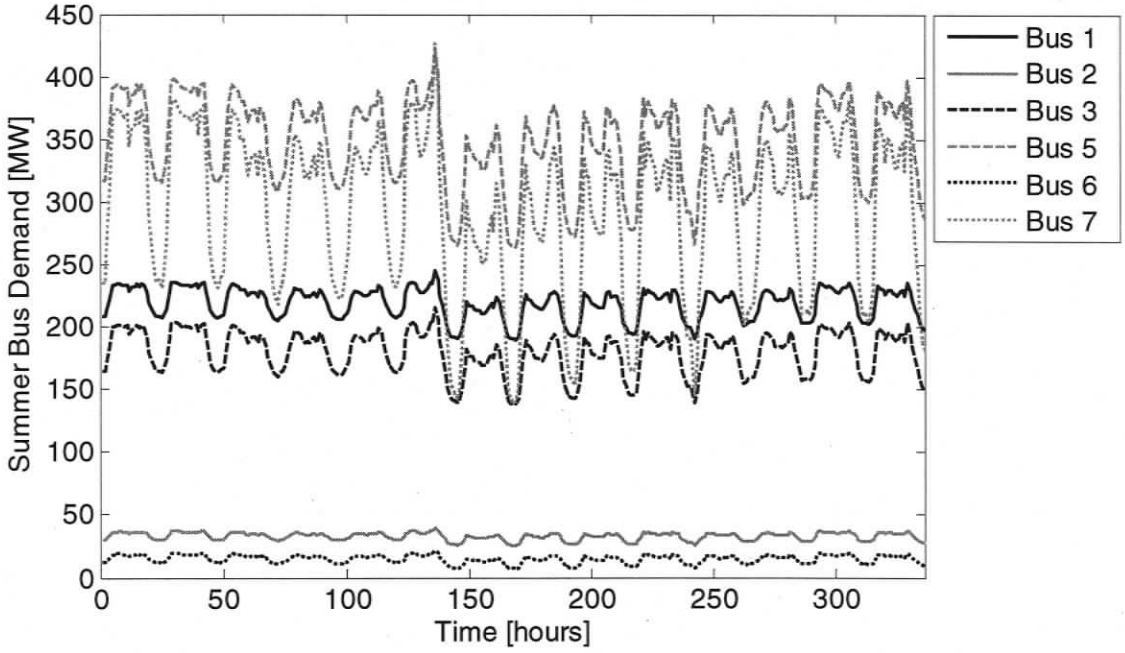

Figure 9. The two week summer demand for each consumer bus.

The dispersion of Island residential and commercial demand among the six Island buses is performed using population and proximity of local substations to each of the buses. Industrial demand was nearly constant at 370 MW, mostly from Island pulp mills, and was dispersed among the six buses according to the proximity of industrial facilities to the buses.

6.2 Generator Ramp Constraints

All thermal and nuclear generators are modeled with ramp rate constraints. The coal and nuclear facilities are modeled to be the most heavily constrained, with a full ramp up time ($\Delta t_{RU,full}$) of three hours and a full ramp down time ($\Delta t_{RD,full}$) of three hours. Natural gas and petroleum combined and simple cycle generators are modeled with a full ramp down time of two hours, but can ramp up fully within one hour. Hydroelectric generators are modeled without ramp rate constraints. Ramp rate time constraints are summarized in Table 2.

Table 2. Ramp rate time constraints for modeled generators.

Generator Technology	Ramp up Time ($\Delta t_{RU,full}$) [hr]	Ramp Down Time ($\Delta t_{RD,full}$) [hr]
IGCC	3	3
Nuclear	3	3
NG CC	1	2
NG SC	1	2
Petroleum CC	1	2
Hydro	1	1

6.3 Operating Costs

The constants $A_{d,c}$, $B_{d,c}$ and $C_{d,c}$ in Equation (14) that describe the variable cost of the dispatchable generators are listed in Table 3. Natural gas [31], coal [32] and

petroleum [33] spot prices are used to calculate $A_{d,c}$ and $B_{d,c}$, and have values of 8.62 CAD/GJ (8.00 USD/MMBtu), 1.53 CAD/GJ (1.42 USD/MMBtu) and 13.03 CAD/GJ (12.08 USD/MMBtu), respectively[2]. A CAD/USD conversion ratio of 0.879275 is used for all monetary value conversions.

Table 3. Fuel and operating and maintenance cost coefficients for dispatchable generators.

Generator Technology	$A_{d,c}$ **[CAD/MWh]**	$B_{d,c}$ **[CAD/MWh]**	$C_{d,c}$ **[CAD/MWh]**
NG CC	-65.12	125.28	2.14
NG SC	-128.12	213.15	3.70
Petroleum CC	-103.12	196.58	2.14
IGCC	-43.50	80.00	3.01
US Average Nuclear	0.00	23.88	0.00
BC Average Hydro	-0.043	1.137	1.60
Southern VI Hydro	-0.021	1.111	1.60
Mid-VI Hydro	-0.035	1.128	1.60
Northern VI Hydro	-0.086	1.189	1.60

Hydrocarbon fuel cost per unit energy is used in conjunction with part load efficiencies for the various technologies to approximate a variable fuel cost with respect to generator part load. Natural gas (NG) simple-cycle and combined–cycle (CC) part load efficiencies are taken from [34] and [35]; with the part load efficiency curve for the NG CC used for the petroleum CC technology. A peak thermal efficiency of 41.1% for an IGCC (Integrated coal-Gasification Combined Cycle) facility is taken from [34], then assumed to decline linearly to 5% when operating at zero part load. The process

[2] The generator cost constants ($A_{d,c}$ and $B_{d,c}$) linearly approximate a cost function for each generator. A cost function is calculated using a series of efficiencies for a generator over its range of part load, and a cost value for a unit of input fuel energy. For example, if a generator is at 50% efficiency, then it requires two units of input energy to produce one unit of output energy. It then takes the cost [CAD] of two units of input energy to produce one unit of output energy [MWh] at an efficiency of 50%. A series of these specific costs [CAD/MWh] are then calculated over the generator's range of efficiency and create the cost function.

undertaken to produce the $A_{d,c}$ and $B_{d,c}$ coefficients for a natural gas combined cycle facility is described in detail in Appendix A.1.

Nuclear cost is modeled as constant, irrespective of part load operating level. Fuel and O&M costs [36] are assumed to be 6.63 CAD/GJ (6.15 USD/MMBtu), and include uranium cost, fuel preparation, O&M, and provision for spent fuel. The cost of 6.63 CAD/GJ represents an average cost for U.S. nuclear facilities [36].

For the hydroelectric facilities, the constants $A_{d,c}$ and $B_{d,c}$ are calculated using water license rental rates associated with power production for 2006 [37], which can be regarded as fuel costs. The rental rates are 1.086 CAD per generated MWh, and 0.006 CAD per 1000 m^3 of throughput water. These dollar amounts are used in conjunction with part load efficiency data for a Francis hydroelectric turbine [38] to approximate variable fuel cost over a range of part load efficiency. Specific head heights and maximum flow rates for Vancouver Island reservoirs are used to calculate the constants for specific Vancouver Island facilities. For hydroelectric costs for generating mixtures other than Vancouver Island, an average head height and maximum flow rate taken from an average of British Columbia mainland reservoirs are used. The process undertaken to produce the $A_{d,c}$ and $B_{d,c}$ coefficients for the BC average hydro facility is described in detail in Appendix A.2.

The constant $C_{d,c}$ represents variable O&M costs, and is taken from [34] for all natural gas, petroleum and coal facilities. The constant $C_{d,c}$ is assumed to be zero for nuclear facilities, since O&M costs are included in the value of $B_{d,c}$. Variable O&M cost for hydroelectric facilities is taken from an Idaho National Engineering and

Environmental Laboratory report [39], and represents an average value for facilities with capacities between 100 and 1000 MW.

The cost for each generator type is plotted together in Figure 10, with the inclusion of both fuel and O&M costs. Figure 10 allows the visual cost comparison of the various generator technologies.

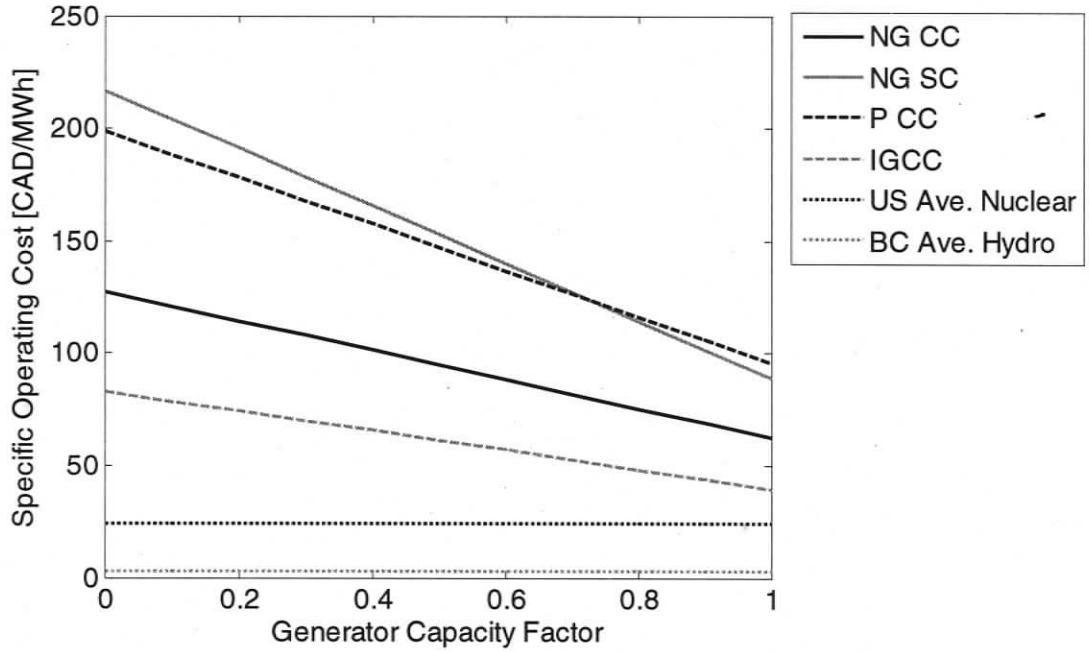

Figure 10. Specific cost curves over the range of generator capacity factor for the various generation technologies.

6.4 Operating Emissions

The constants $A_{d,e}$ and $B_{d,e}$ (Equation 16) that describe the variable emissions of hydrocarbon fed generators are listed in Table 4. The carbon dioxide equivalent emission factors [34] used to calculate $A_{d,e}$ and $B_{d,e}$ correspond to fuel grade natural gas, average U.S. electric utility coal, and motor gasoline petroleum. A petroleum fueled facility

would typically not combust engine grade gasoline, likely combusting diesel instead, but an emissions factor for gasoline was used, and would not be far from the emissions associated with diesel combustion. The actual emission profiles for the hydrocarbon fed generators are nonlinear, and the values of $A_{d,e}$ and $B_{d,e}$ linearly approximate these profiles. The coefficients associated with emissions are calculated using the same method that was used to calculated the cost coefficients: using a series of efficiencies and the emissions per amount of required input energy into the generator to produce one unit of output energy.

Table 4. Carbon dioxide equivalent emission coefficients for hydrocarbon fed generators.

Generator Technology	$A_{d,e}$ **[kg CO_2e/MWh]**	$B_{d,e}$ **[kg CO_2e/MWh]**
NG CC	-381.88	727.96
NG SC	-744.47	1238.50
Petroleum CC	-525.34	1001.40
IGCC	-5000.00	6000.00

6.5 Available Wind Power

Bus 2 encompasses the non-dispatchable generator, simulating multiple wind turbines at a single location. The 336 data points (hourly wind speed over two weeks) used for this exercise were observed at Jordan Ridge on Vancouver Island (Lat: 48 25 48, Long: -124 03 45) from August 19 to September 1, 2001, at a height of 30 m above the site elevation of 671 m [40]. This two-week wind profile was chosen because it includes both maximum and minimum annual wind speeds. Measured wind speeds at this location are indicated in Figure 11, as is the power generated from a single Enercon 70 wind turbine. The wind speed is measured at 30 m, but was scaled to correspond to a turbine hub height of 113 m.

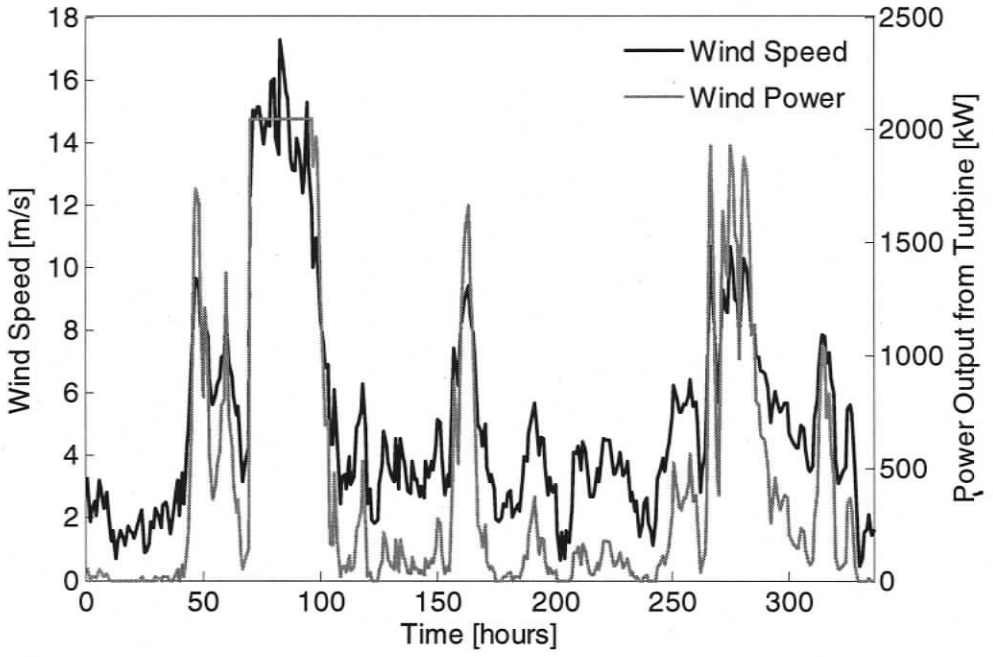

Figure 11. Two week wind profile at Jordan Ridge and the associated power profile from an Enercon E70 turbine.

All simulation results presented in this paper, for both Summer and Winter demand periods, will use the same two week wind profile in order to facilitate better comparisons among all the scenarios. Wind generation is modeled with zero cost, although some analyses will include an amortized capital cost of the wind farm installation.

6.6 Transmission Constraints

Each of the nine bus connections (*a* through *i*) of the simulated network have a constraint placed on the amount of power that can be sent across them. Three cable constraint scenarios have been created – unconstrained, constrained and actual constraint

cases. The cable capacities for each cable and each of the three scenarios are listed in Table 5. For all constraint cases, the transmission capacity on cable *d* is 1300 MW, representing the actual transmission capacity of the submarine cable connecting Vancouver Island to the BC mainland. For the unconstrained scenario, all cable capacities are set to 2000 MW except for cable *d*. Cables *a* and *c* connect the wind farm to the network; if the peak power generation from the wind farm exceeds 2000 MW, the capacities on these two cables are set to the peak wind farm output plus 20%. The constrained scenario uses actual cable capacities for the Vancouver Island grid, with the same variable capacity criteria set out for cables *a* and *c*. The actual constraint scenario again uses the actual cable capacities for the Vancouver Island grid, but now the capacities of cables *a* and *c* stay constant at 60 and 100 MW, respectively. The network connections are constrained for initial Vancouver Island results, but are relaxed when comparing various generation mixtures.

Table 5. Network connection capacities for three constraint scenarios.

	Cable Capacities [MW]		
Cable	**Unconstrained**	**Constrained**	**Actual**
a	2000 or higher	60 or higher	60
b	2000	320	320
c	2000 or higher	100 or higher	100
d	1300	1300	1300
e	2000	700	700
f	2000	610	610
g	2000	300	300
h	2000	650	650
i	2000	650	650

6.7 Penalty Value Associated with Power Transmission

Equation (15) shows the objective function of the network optimization with a cost associated with power transmission. The use of a penalty value (PV) is employed to assign a certain level of transmission cost to the objective. If too large a penalty value is used, then the optimization will not focus on an optimized operating cost scenario, as is desired. If too small a penalty value is used, then transmission will have a negligible impact on the objective function, and transmission levels will be disregarded. A sensitivity analysis was performed that reduced the penalty value by factors of ten from 10^{-2} to 10^{-8} to examine the effect of the value on the objective function and solution vector.

The US aggregate mixture with 50% wind penetration, winter demand, and no transmission constraints was used to analyze the effects of all penalty values. With penalty values greater than 10^{-2}, the optimization process failed to converge to a solution, irrespective of algorithm start point. At a penalty value of 10^{-2}, the optimization converged to a solution for roughly 1% of random start points. At a value of 10^{-3}, the optimization converged to a solution for roughly 80% of random start points. At values of 10^{-4} and less, the optimization converged to a solution irrespective of algorithm start point.

Figure 12 shows the difference between the two objective functions (15) and (13), with *Cost* referring to just the operating cost of generators (Equation 13), and $Cost_{PV}$ referring to the value of both operating and transmission costs (Equation 15). The ordinate axis of Figure 12 shows this difference ($Cost_{PV} - Cost$) as a ratio over the cost without the transmission penalty ($(Cost_{PV} - Cost)/Cost$); this decimal value is then expressed as a percentage. At a penalty value of 10^{-2}, the composite value of the objective

from transmission is 25% of that of the cost due to generator operation. As the penalty value is reduced to 10^{-5}, the transmission contribution to the objective is reduced to below 1% of the operating cost contribution.

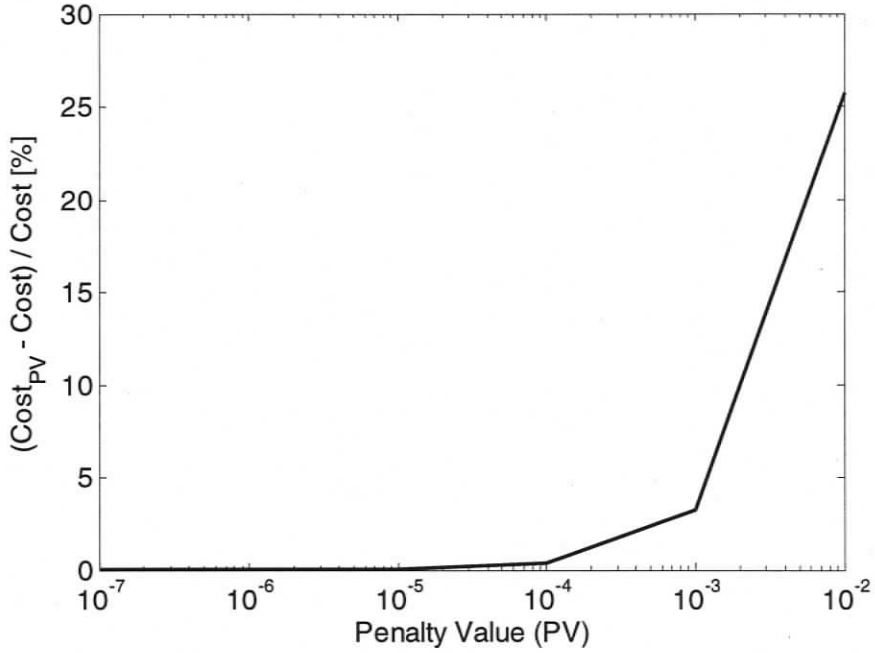

Figure 12. Convergence of the objective function with and without the transmission penalty for various penalty values.

From these results, a penalty value of 10^{-4} was chosen to assign a cost to power transmission. This value provides optimal solutions irrespective of algorithm start point, and scales the transmission contribution to the objective to roughly 1% of the contribution due to operating cost; a suitable contribution that does not significantly alter the original objective value. All results seen in this thesis correspond to a penalty value of 10^{-4}.

7. Results and Discussion

Unless otherwise indicated, all results are based on the existing generation mixture on Vancouver Island.

7.1 Optimal Power Flow Results

Wind power penetration is used to measure the growth of a wind farm installation. It is defined as the wind farm's name-plate capacity normalized with respect to peak network demand, which is 1971 MW for the simulated network. For example, a 10% wind power penetration implies a wind farm capacity of 197.1 MW, or 96 installed Enercon E70 turbines rated at 2.05 MW each. Two forms of wind penetration into a network can occur: power penetration and energy penetration. Power penetration is a measure of the instantaneous peak power that enters a network at a given time, while energy penetration is a measure of how much wind energy enters a network over a specified period.

The maximum allowable power penetration entering the network depends on the cable capacities that link the wind farm to the network, as well as on the demand at the bus where the wind farm is located. The amount of power transmitted to or from the bus where the wind farm is located is that which remains after the local demand has been subtracted from the wind generation (positive outgoing and negative incoming). A large demand at the wind farm bus will allow a larger power penetration, if the periods of high demand and high wind generation coincide. For the winter demand profile, wind power penetration can rise to 9.9% for the actual constrained scenario, and 127.3% for both the unconstrained and constrained scenarios. For the summer demand profile, wind power

penetration can rise to 9.6% for the actual constrained scenario, and 113.2% for both the unconstrained and constrained scenarios. The low penetration for the actual cable capacities scenario exemplifies the need for additional transmission capacity if wind power penetration into the network is to exceed 10%.

The *energetic capacity factor* is a ratio of produced energy over a given time period divided by the maximum amount of energy that that capacity could provide over the same time period. The wind profile has an energetic capacity factor of 22.7% over the two winter weeks considered in the model. If truncation of wind generation is allowed, a higher amount of wind energy can be introduced into the network without raising transmission capacities; however, truncation will result in a drop in the capacity factor of the wind farm. The energetic capacity factor for the wind farm is shown in Figure 13 with respect to increasing wind power penetration (using the cable capacities of the actual constraint circumstance and the winter demand profile). As wind penetration increases to roughly 10%, the capacity factor stays constant at 22.7%, and no truncation of wind generation is required. Once the output of the wind farm reaches the limit of the cables connecting it to the network, a portion of the generation must be truncated and the capacity factor drops. Two capacity factor curves, one corresponding to a 100 MW capacity on cable c and the other to a 200 MW capacity on cable c, are shown in Figure 13. When the capacity of the cable connecting the wind farm to the grid is raised, a larger portion of the wind energy can enter the network, resulting in larger energetic capacity factors, seen by the difference between the two curves in Figure 13.

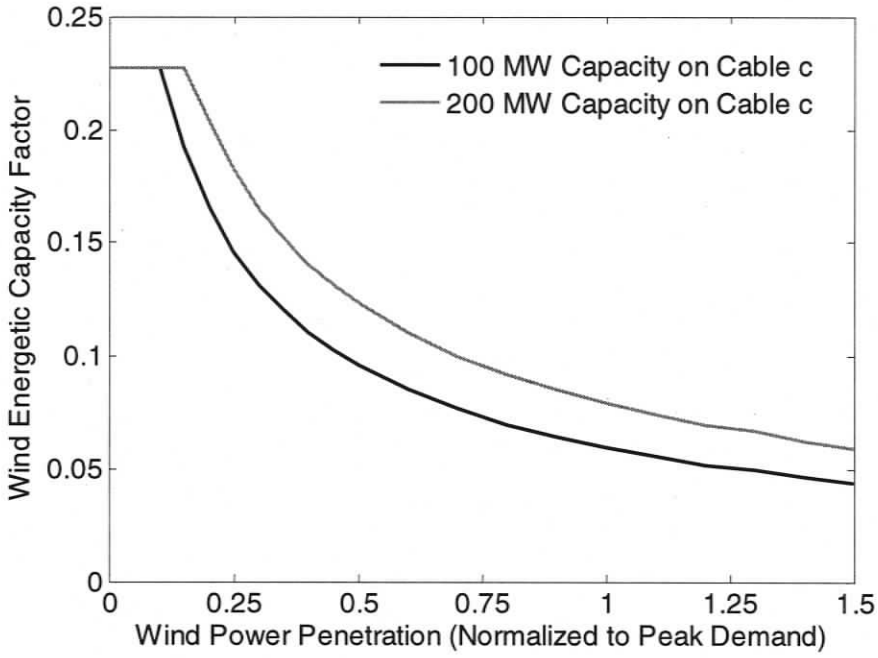

Figure 13. The reduction of wind farm capacity factor due to transmission constraints forcing wind power truncation.

The demand profiles for the network are less variable than the wind generation profile, with an average power demand of 76.7% of the maximum of 1971 MW during the winter period, and an average power demand of 79.4% of the maximum of 1372 MW during the summer period. A highly intermittent source partially supplying power for a more regular demand results in the existing generators in the network ramping up and down more frequently to balance the remaining load; this results in a drop in the capacity factors for the existing generators as the size of the wind farm grows (see Figure 14). The existing dispatchable generators are modeled to have a higher cost at lower capacity. Therefore, a drop in the capacity factor directly increases the operating cost of the generators. The two thermal generators show a smooth decline in capacity factor with increased wind penetration. The most expensive generator, the natural gas simple cycle

(NGSC), has the lowest capacity factors (maximum of 10%), due to the solver minimizing the use of the highest cost generator. The natural gas combined cycle (NGCC) generator has a lower operating cost than the NGSC generator, and is used more frequently, with a maximum capacity factor of 50% at zero wind penetration. The four hydro generators are used at the highest capacities, due to their costs being less than 5% of that of the NGCC generator. It can be seen in Figure 14 that the capacity factors of the four hydro facilities behave sporadically as wind penetration grows, with jumps of more than 30% capacity factor for a difference of 10% wind power penetration. This erratic behaviour is due to the small difference in operating cost between the four facilities. On the scale of total system cost over 336 hours, the solver does not differentiate the benefit of running one hydro generator before another, and thus the usage of the hydro generators are exchanged for the various solutions. If the four hydro generators are considered as one, with the full capacity being the sum of the individual capacities, then the combined hydro generator shows a smooth decline in capacity factor as wind penetration grows. This is shown with the "Combined Hydro" trend in Figure 14, where capacity factor results correspond to the winter demand profile and relaxed transmission constraints.

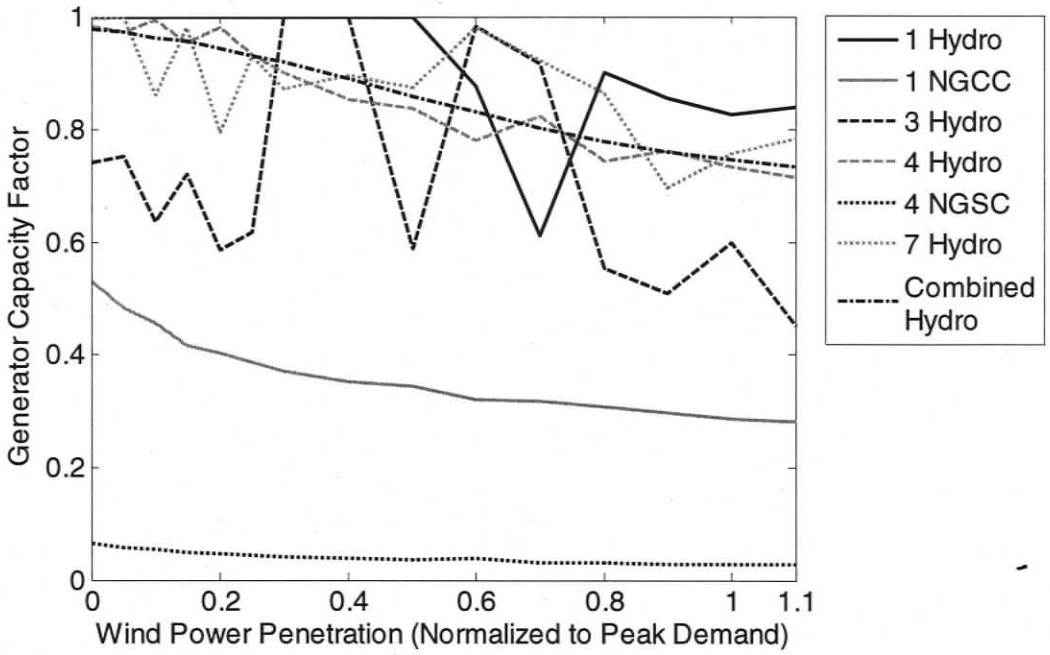

Figure 14. Average capacity factor as a function of increasing wind penetration for the various generators in the Vancouver Island mixture.

A load duration curve (LDC) is constructed by sorting demand over a certain period from maximum to minimum, thereby identifying the portion of demand that can be met by base load. Base load is the portion of demand that remains constant throughout the period, with variations above base load demand to be met by load following or peaking generation sources. As wind penetration grows, the base load component of the network demand decreases, which can reduce the amount of time an existing generator can operate at a steady output. Six LDCs for winter and one for summer demand are shown in Figure 15. Different amounts of wind generation are subtracted from demand in the construction of the LDCs.

The 'no wind' LDC shows the unreduced demand for the winter period, with a base load of approximately 1000 MW. As wind penetration increases, more of the

demand is satisfied with wind power, but the base load requirement falls. At 60% wind penetration, the base load requirement drops to zero, and the opportunity for a generator to remain at a constant generation level over the two-week period is eliminated. At penetrations above 60%, the LDCs become negative at the tail end of the duration, indicating that generation from the wind farm has exceeded demand and that export of power out of the network must occur. When demand is low and wind penetration is high, more excess wind generation occurs and a larger proportion must be exported, which is shown by the 100% wind penetration for the summer demand LDC (Figure 15).

Figures 14 and 15 together show the decline of base load demand with increased wind penetration, which forces a drop in capacity factors for most generators. This in turn results in an increase in the operating cost of existing generators. The induced cost on existing generators from wind's variability will be discussed next.

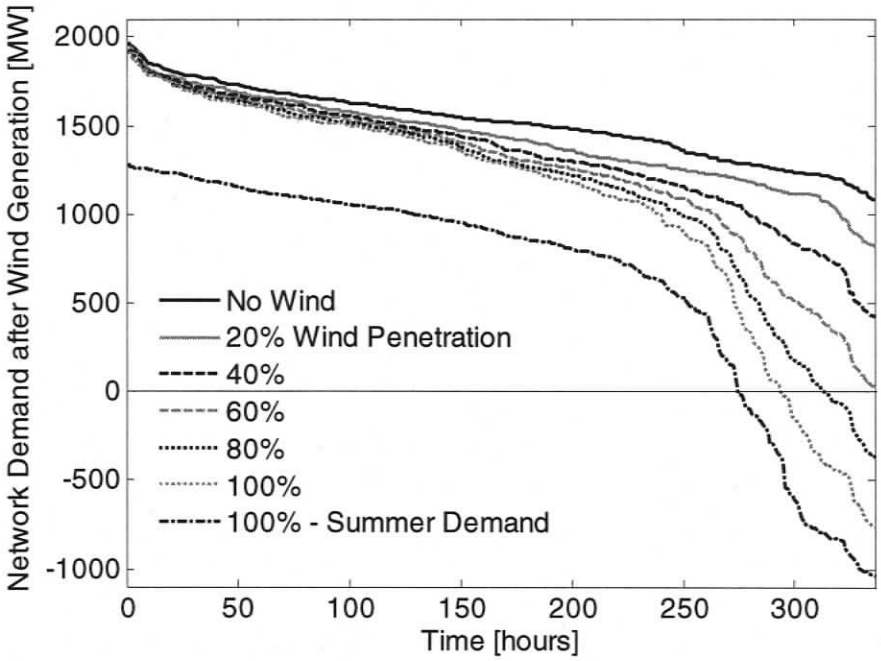

Figure 15. Load duration curves after increasing amounts of wind power has been subtracted from demand.

7.2 Wind Induced Cost on Existing Generators

The combined hydro generator consisting of the sum of the Vancouver Island hydro facilities is used to illustrate the effect that the introduction of wind-generated power has on the operating costs of existing generators. The combined hydro generator has been modeled to cost a minimum of 1.095 CAD/MWh at full operating capacity (denoted c_{FC}), and a maximum of 1.141 CAD/MWh at zero operating capacity (denoted c_{ZC}). Thus it has a cost range of $c_R = c_{ZC} - c_{FC} = 0.046$ CAD/MWh. The average cost of the generator with wind penetrating the network can then be defined incrementally as a percentage of the cost range:

$$\overline{c}_I \equiv \frac{\overline{c}_W - \overline{c}_o}{c_R} \tag{19}$$

where $\overline{c}_I$ is the average incremental cost of the existing generator, $\overline{c}_W$ is the average cost of the generator with wind penetration (a function of wind penetration) and $\overline{c}_o$ is the average cost of the generator without any wind penetration. These costs and their range are small compared to the costs of a natural gas facility, but, by presenting results as a percentage of the cost range, it is still possible to provide insights into the potential increase in operating costs induced by wind penetration. The average incremental cost, $\overline{c}_I$, for the combined hydro generator is shown in Figure 16 with respect to increasing wind power penetration.

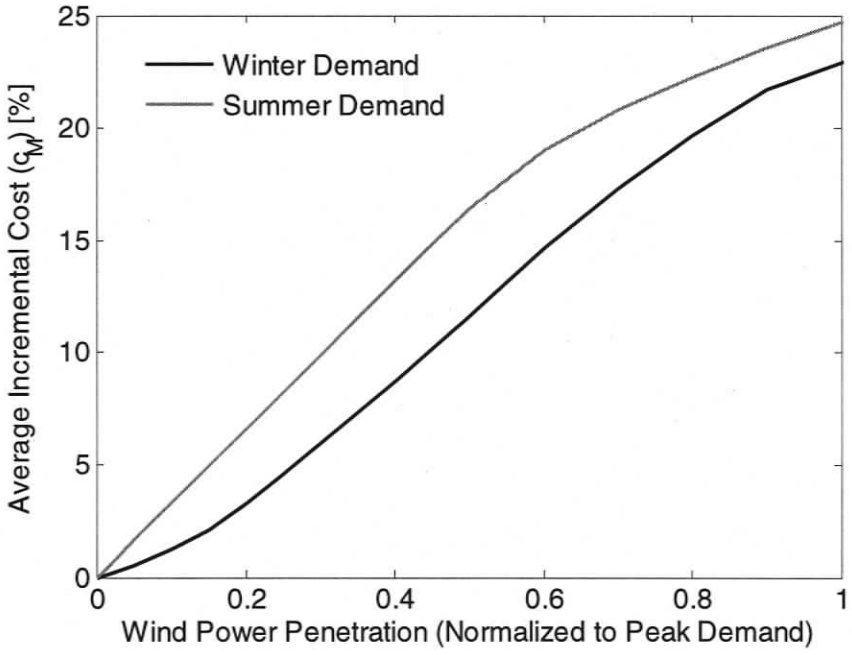

Figure 16. Increase in average operating cost of all the hydro generators induced by wind intermittency.

The incremental cost is zero when no wind power enters the network. As wind penetration grows to 100% penetration, the incremental cost of the hydro generator rises

to 25% of the full cost range. The induced incremental cost for the summer demand profile is larger than the induced cost for the winter profile due to less power absorption buffering the intermittency of the wind source in the network and because a lower capacity factor is expected of a generator during periods of low demand. When demand drops and wind generation remains the same, the capacity factors of existing generators drop further compared to high demand periods, resulting in greater variance and a higher operating cost. This is shown by the difference between the two curves in Figure 16.

7.3 Wind Penetration Effects on the Vancouver Island Generation Mixture, System Costs and CO_2 Emissions

What happens to system costs as wind penetration grows? If per unit operating costs of generators do not increase as output falls relative to capacity, one would expect total system operating costs to decline linearly as wind penetration grows and wind power satisfies at zero cost the demand previously satisfied by existing generators. This is not the case, however, for at least two reasons. First, ramping constraints prevent thermal power plants from responding quickly enough to the availability of wind power to the grid. Second, as wind penetration grows, the costs of using extant generators to satisfy remaining demand rises, so system-wide costs decline at a declining rate, as illustrated in Figure 17. The data in Figure 17 correspond to the winter demand profile and a lack of constraints placed on the network transmission cables. A certain cost to operate the system exists at zero wind penetration, where the entire demand is met by existing generators (12.5 CAD/MWh). As wind penetration grows, a portion of the demand previously met by existing generation is now satisfied by zero cost wind and the total system operating cost declines. As wind penetration becomes increasingly significant, the

induced intermittency on existing generators also grows, increasing their specific cost and diminishing the benefit of introducing the large wind farm. However, all this ignores capital costs.

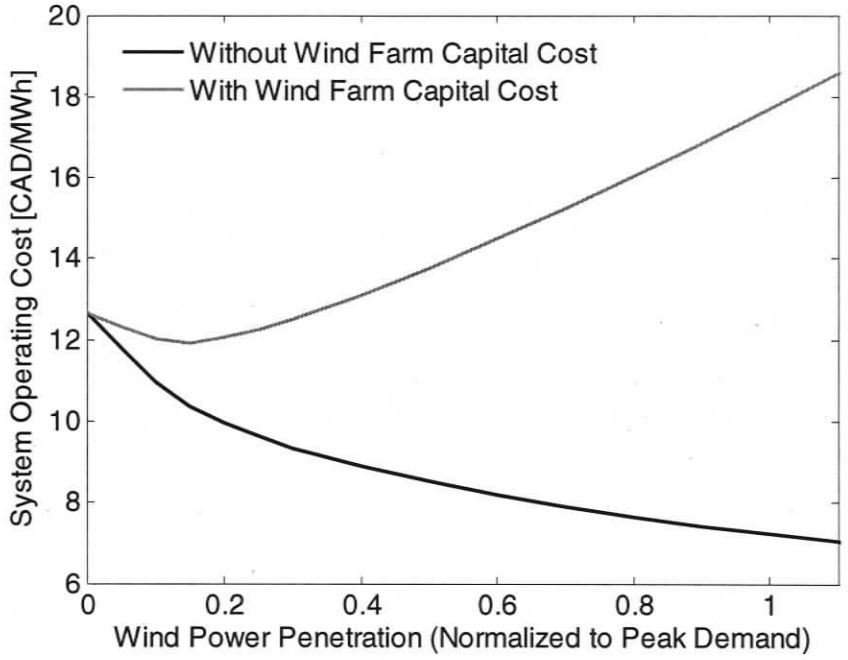

Figure 17. Vancouver Island system operating cost, with and without an amortized capital cost for the wind farm.

If capital costs related to the construction and installation of the wind farm are taken into account, total system operating cost declines initially, but then grows above zero wind cost as penetration exceeds 30%, as also indicated in Figure 17. The capital cost for the wind farm is assumed to be 600 CAD per kW of installed wind capacity [5], and is amortized over 20 years at a discount rate of 10%. The annual amortized fee is then reduced by a fraction of (336/8760) to approximate a two-week amortized capital cost for the wind farm construction and installation. Including capital costs causes total

system operating costs to decline by 5% at a penetration of 15%, but then causes cost to increase by almost 50% as wind penetration reaches 110%, compared to a cost decline of almost 50% at 110% penetration if capital costs are ignored.

When the capital cost of the wind farm installation is included, the increase in overall system operating cost indicates that adding wind capacity beyond 30% penetration can be distinctly detrimental. This can be partly attributed to the inexpensive existing generation mix for the network. A typical North American generating mix is predominantly thermal [34], unlike on Vancouver Island where hydroelectric dominates, supplying 70% of peak load. When considering fuel costs for a thermal-dominated generation mix, overall system operating cost will be significantly larger and the economic benefit of adding wind capacity to the system will be greater than indicated in Figure 17. The consideration of wind penetration with different generation mixtures will be discussed in section 7.4.

System emissions should also linearly decline with increasing wind penetration if existing generator environmental performance did not alter with respect to their part load, and ramp rate restrictions were not included. This is not the case, however and, as the capacity factors of the thermal generators in the network decline, their emissions per unit output increase. The trend of system emissions, in kilograms of carbon dioxide equivalent per MWh, with respect to increasing wind penetration is shown in Figure 18, where the decline of system emissions at a declining rate is illustrated.

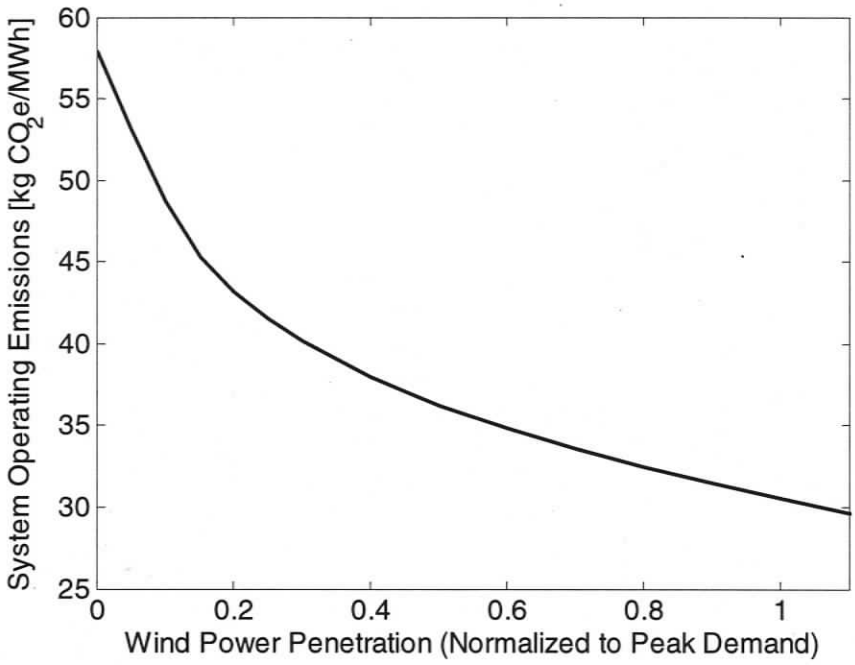

Figure 18. Vancouver Island system operating emissions for a range of wind penetrations.

System emissions for zero wind penetration are low (58 kg CO_2e/MWh) for Vancouver Island compared to other thermal dominated mixtures; a comparison of environmental performance for different regions is presented in Section 7.4. Emissions are low due to the large percentage of zero emission hydroelectric facilities meeting demand on Vancouver Island. The carbon emitting thermal generators are the most expensive for the Vancouver Island mixture, and thus wind generation replaces thermal generation first with an optimum economic dispatch objective, leading to a sharp initial reduction of produced carbon dioxide at low wind penetrations. As wind penetration grows to 110%, emissions continue to decline more than 50%, but at a declining rate. This occurs for two reasons: the emissions per unit output of the thermal generators increase as wind penetration increases, and the replacement of thermal capacity lessens

for large penetrations, as wind replaces all thermal and begins to replace zero emission hydroelectric capacity.

7.4 Wind Penetration Effects on Various Generation Mixtures

7.4.1 System Costs and Network Export

For results shown throughout the remaining sections of the thesis, constraints on the power flows across network cables have been removed. The motives of comparing various generation mixtures are not focused on the optimization of a constrained network, and focus more on cost and emission tradeoffs of wind integrating with various capacities of different generating technologies.

This section discusses wind penetration into five different generation mixtures: the Vancouver Island mix (VI) considered earlier, the Canada aggregate (CAN), the United States aggregate (US), the Northwest Power Pool of the United States (NWPP), and the Mid-America Interconnected Network of the United States (MAIN). Again, for each generation mixture, the transmission and power grid of Figure 5 is employed. System operating cost for each of the five mixtures is shown in Figure 19 with respect to a range of increasing wind penetration.

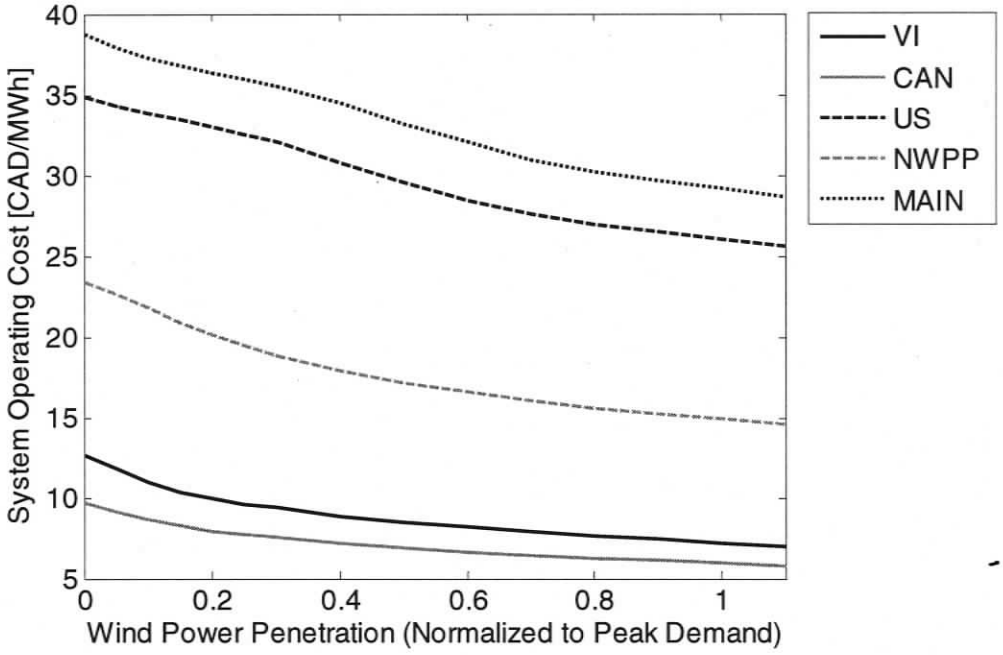

Figure 19. System operating cost for the five simulated mixtures.

System operating cost at zero wind penetration for the VI mix was previously shown to be 12.5 CAD/MWh, among the lowest in North American (Figure 19). The NWPP, US and MAIN mixtures all exceed the VI operating cost at zero wind penetration, with values of 24, 35 and 39 CAD/MWh, respectively. The increase in zero wind operating cost for these three regions occurs because of the large percentage of high cost thermal generation compared to the VI mix. The US and MAIN mixtures have zero wind costs that are roughly three times greater than the VI cost, with both mixtures having less than 10% of their capacity as hydroelectric, and the majority of their capacity coming from coal, natural gas and nuclear sources. The zero wind operating cost for the CAN mix falls below the VI cost. Both mixtures have a large percentage of hydro capacity (10% less for the CAN mix), but the CAN breakdown replaces a portion of the

natural gas capacity seen in the VI mix with less costly nuclear capacity, resulting in a lower overall variable cost.

All mixtures show a reduction in system operating cost for the range of wind penetration up to 110%. The extent to which the cost is reduced is shown in Figure 20, where the incremental operating cost for each mixture is presented. The incremental cost for a specific mixture is calculated by subtracting the zero wind cost from the cost at each level of wind penetration. Thus at zero wind penetration, incremental cost is zero. Figure 20 compares the operating cost reduction between the various mixtures on the same scale, irrespective of the large differences seen in the absolute cost curves in Figure 19.

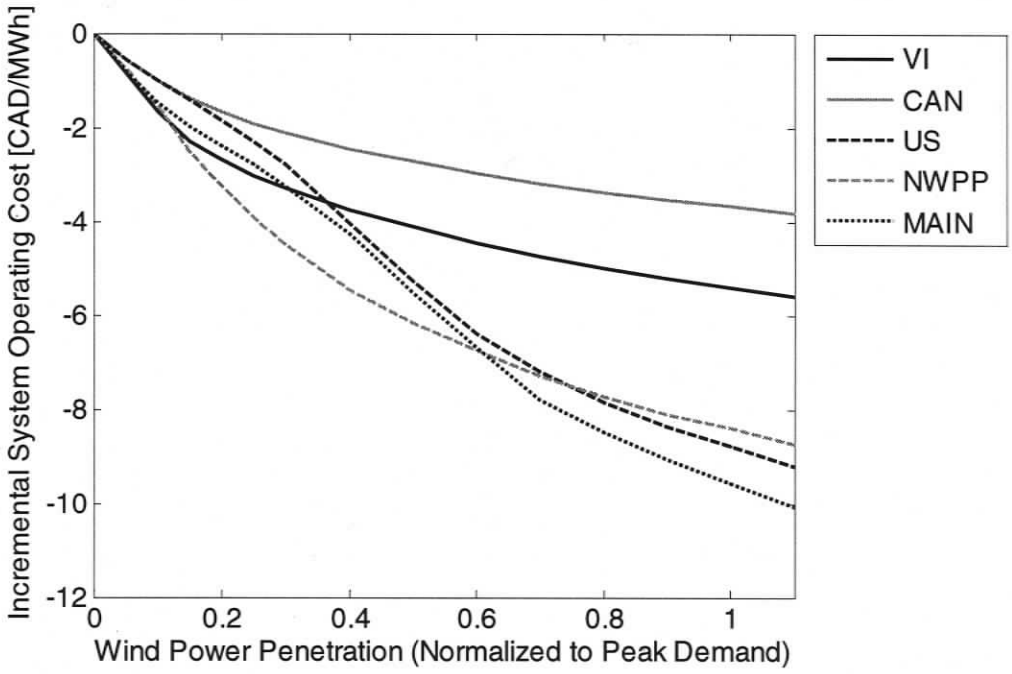

Figure 20. Incremental system operating cost (compared to zero wind cost) for the five simulated mixtures.

The incremental cost values seen in Figure 20 are all negative, showing a reduction in operating cost for the full range of penetration for all mixtures. Thermal dominated

mixtures (US, NWPP, MAIN) show the largest decline of 8 - 10 CAD/MWh, with wind replacing more expensive generation compared to the mixtures with a large portion of inexpensive hydroelectric and nuclear capacities.

Before the incremental cost curves in Figure 20 are discussed further, it is helpful to consider the level of ramp constrained capacity for the various mixtures. The pie charts shown in Figure 21 indicate the percentage of capacity that has a certain level of ramping restriction placed on it. Three levels of ramp constraints are shown: high refers to coal and nuclear facilities that can only ramp up and down one third of their capacity during one hour, medium refers to natural gas and petroleum combined and simple cycles that can ramp up fully within one hour but can only ramp down half their capacity in one hour, and low refers to hydroelectric facilities that are not ramp constrained. For example, the NWPP mixture has 18% of its capacity that is highly ramped constrained, 39% that is constrained at a medium level, and 43% of low constrained capacity. The US and MAIN mixtures are quite distinct from the other mixtures, with 70% of their capacity being highly ramp constrained and less than 10% having no ramp constraints.

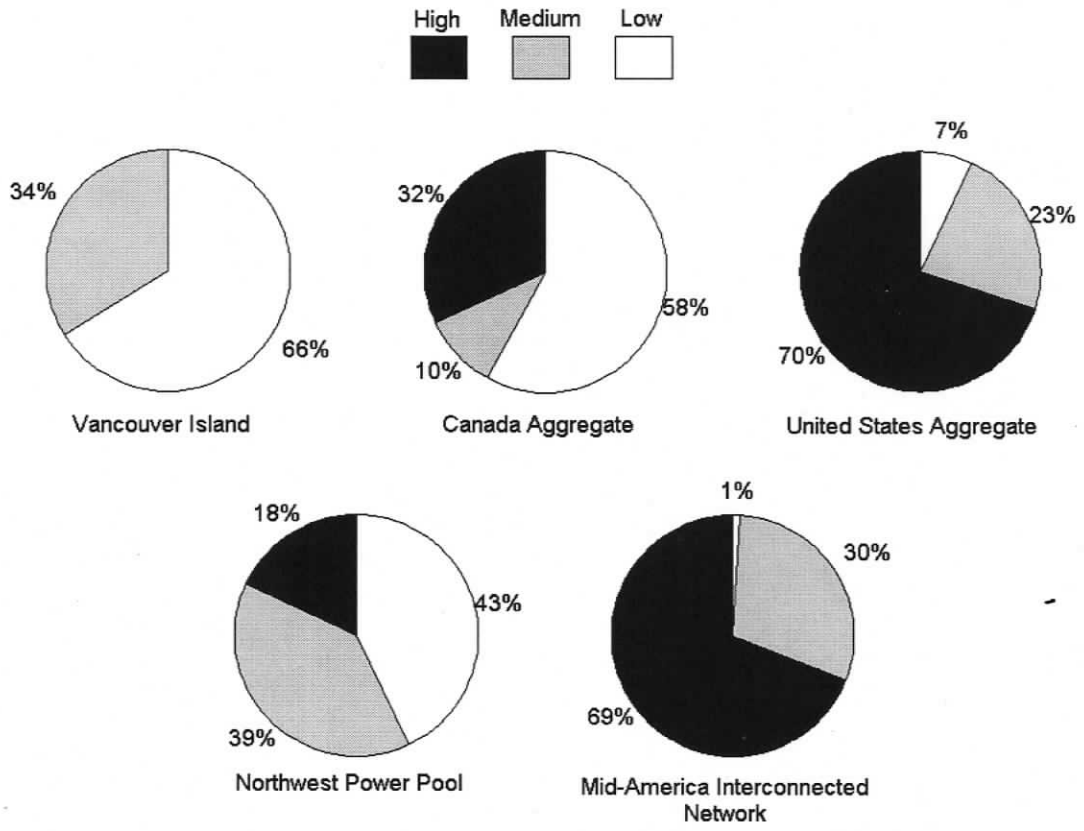

Figure 21. The level and percentage of ramp constrained capacity for each mixture.

With the aid of Figure 21, the level at which each mixture is ramp constrained is identified, and a more in depth consideration of Figure 20 can now occur. The two mixtures, US and MAIN, do not show a smooth decline in operating cost in Figure 20. This uneven feature is due to the high ramp constraints placed on those mixtures. Excess generation occurs if generators are not able to ramp down fast enough when wind power quickly spikes, thus costing the system more than would occur if the generators were able to ramp down quickly to just meet demand. The other three mixtures, VI, CAN and NWPP are not as highly ramp constrained (Figure 21), and wind penetration results in smooth cost reductions (Figure 20). The Canada aggregate mixture shows the smallest cost reduction for all the mixtures. The introduction of zero cost wind is not able to

significantly reduce the cost of the CAN mix because the mix is already inexpensive without wind. Uneven trends arising from excess generation due to wind intermittency and high ramp constraints will be discussed in more detail when examining power export from the network.

The cost trends shown in Figures 19 and 20 do not include the amortized capital cost of the wind farm. Incremental system operating cost with respect to wind penetration is again shown in Figure 22, now with the inclusion of the wind farm capital cost.

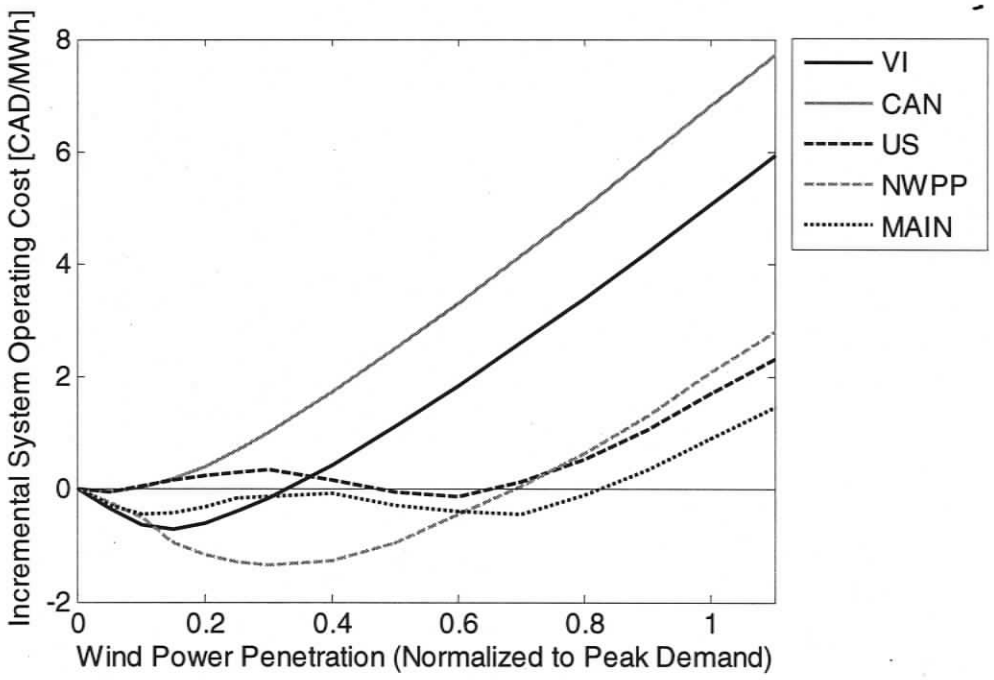

Figure 22. Incremental system operating cost (compared to zero wind cost) for the five mixtures, with an amortized capital cost for the wind farm.

As discussed in the previous section, the VI mixture exhibits a reduction in operating cost when considering wind farm capital up to a penetration of 30%, with the peak cost reduction occurring at 15% penetration. The Canada Aggregate mixture, having

the lowest overall cost and the smallest cost reduction due to wind, shows a negligible cost reduction for penetrations up to 10% and a distinct cost increase for the remaining penetration range.

The uneven cost reduction of the highly ramp constrained mixtures (US and MAIN) was discussed when examining Figure 20. These uneven cost trends are amplified when considering incremental operating cost that includes wind farm capital. The two high ramp constrained mixtures show the tendency to reduce cost for moderate amounts of wind penetration, but ramp constraints force excess generation, raising cost, and yielding positive incremental values for moderate penetrations in the US mix, and slightly negative (-0.5 CAD/MWh) incremental values for moderate penetrations in the MAIN mix. For high wind penetrations, above 80%, both the US and MAIN mixtures show a positive incremental cost, resulting in an increase of operating cost at high penetration.

The NWPP mixture shows the largest cost reduction due to wind penetration into a thermal dominated mixture, without the increase in cost from ramp constrained excess generation. Wind initially replaces high cost thermal generation and system operating costs decline rapidly, similar to the US and MAIN mixtures; but the moderate ramp constraints on the NWPP mix now allows the generators to better follow the wind intermittency and excess generation does not occur in the same amount as in the US and MAIN mixtures. This results in a smooth decline in operating cost, up to a penetration of 30%, where the cost then begins to increase and becomes incrementally positive at a penetration of 70%.

Exported power due to ramp constrained capacity and excess wind generation is shown in Figure 23, where the peak amount of exported power over the two week winter demand is plotted for the various mixtures and range of wind penetration.

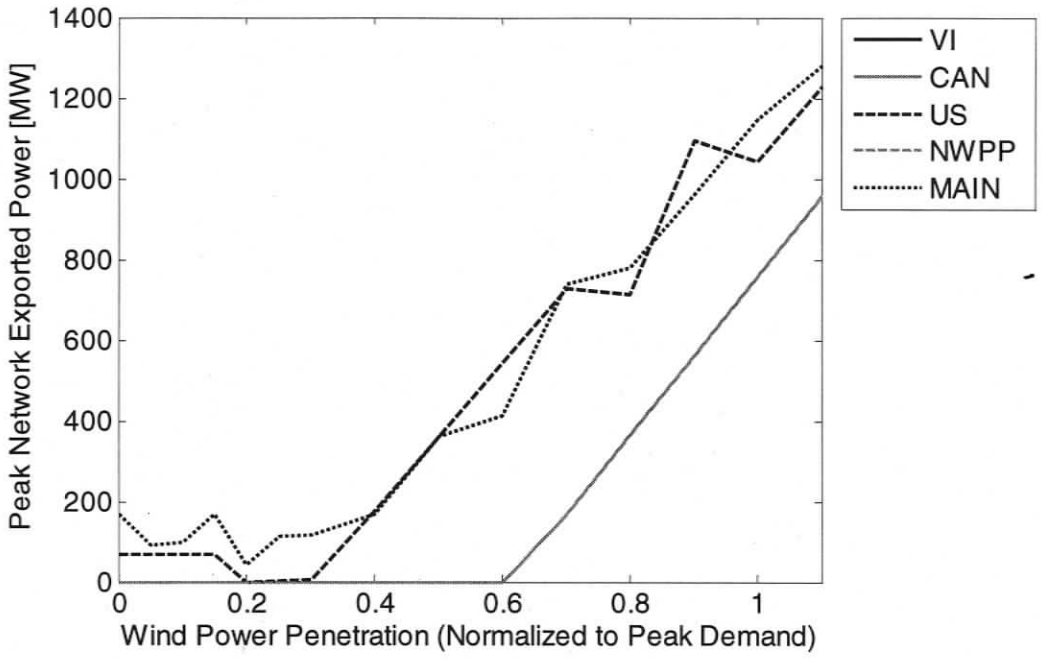

Figure 23. Peak power export from the network for the five mixtures.

The VI, CAN and NWPP peak export trends all fall atop each other, showing the peak export requirement for low and moderately ramp constrained mixtures. The increase in peak export from zero that occurs at 60% penetration for these mixtures is due to wind generation exceeding network demand at certain time periods. As wind penetration exceeds 60%, the amount of excess wind power grows linearly, as does the peak export for the three mixtures (VI, CAN and NWPP). For the two high ramped constrained mixtures (US and MAIN), power export is necessary even when wind penetration does

not exceed network demand - when export is only due to the inability of ramp constrained generators to buffer sudden wind capacity decreases.

Power export for the VI, CAN and NWPP mixtures is due to wind generation exceeding demand, and this can be verified by examining the peak excess wind generation over the range of penetrations (see Figure 24) [3].

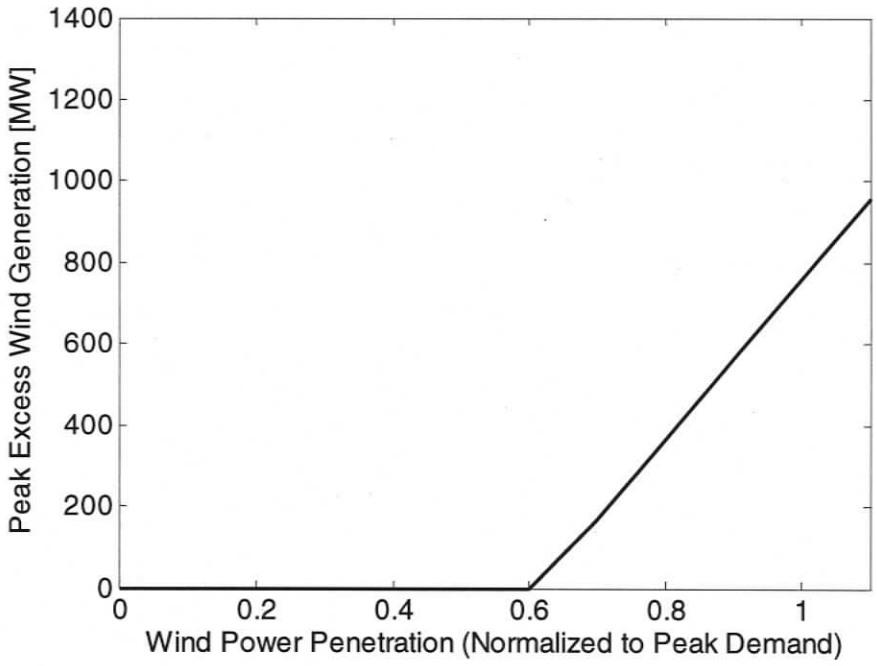

Figure 24. Peak power export from the network due to wind excess only.

The trend of peak excess wind matches the peak power export for the three low ramp constraint mixtures (VI, CAN and NWPP), validating that export from these mixtures is due to wind only, and not from generator ramp restrictions on existing

[3] For the two week winter demand, the chosen wind profile, and penetrations beyond 60%, there exists periods during the 336 hours where wind generation exceeds total network demand. The peak excess wind generation refers to the peak amount of wind generation that goes beyond the total network demand, thus peak excess wind.

capacities. This match also verifies that the difference between the high ramp constrained trends (US and MAIN) and the low ramp constrained trends (VI, CAN and NWPP) in Figure 23 is due to ramp restrictions only. If wind penetration is to occur into a highly ramp constrained generation mixture, then either significant ties to other networks or a method for consuming excess generation must be present to absorb the excess power.

Figure 23 also aids in explaining the uneven trends seen in Figures 20, 21 and 22 for the US and MAIN mixtures, confirming that a significant amount of excess generation does occur in these mixtures due to ramping restrictions, even for low levels of wind penetration.

Wind penetration may seem favorable for a mixture that is hydroelectric dominated, such that existing capacity has the ramping ability to buffer the intermittency introduced by wind. However, on an economic basis, wind penetration exhibits the largest benefit when introduced into a thermal dominated mixture with generators that respond quickly, due to wind replacing expensive thermal capacity (expensive compared to hydro capacity). These results also show that, when including the ramping limitations of thermal facilities, the economic benefit of introducing wind into thermal dominated mixtures may be reduced, due to the cost of excess thermal generation that occurs during fast decreases of wind generation.

7.4.2 System Emissions

The operating emissions for the five simulated regions are shown in Figure 25 over a range of wind penetration up to 110%.

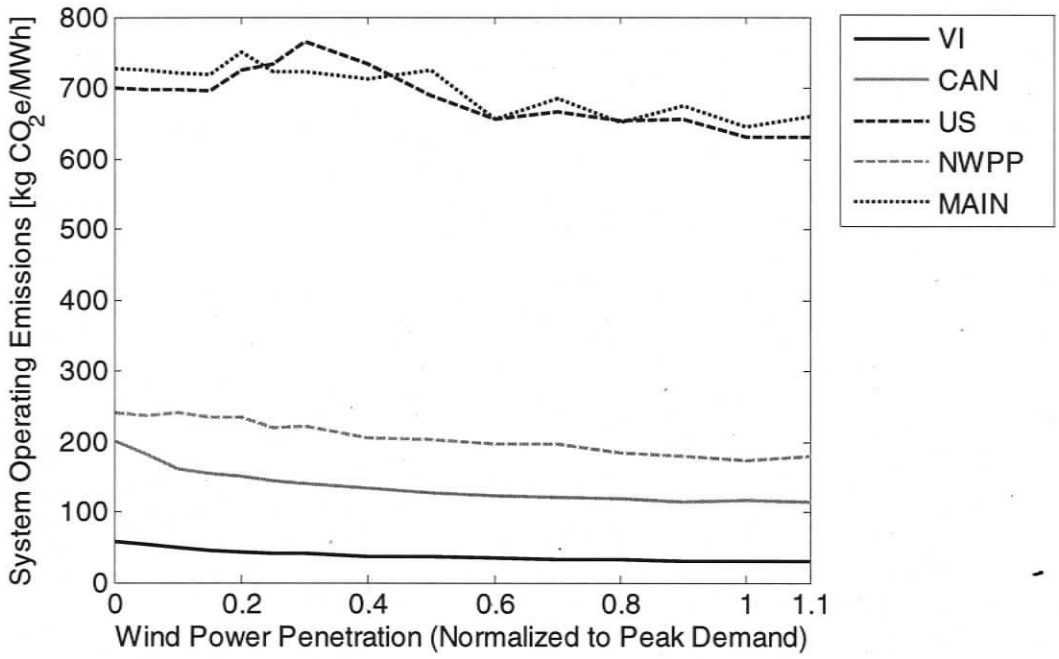

Figure 25. System operating emissions for the five mixtures.

Emissions for the VI mix are low compared to other regions, at 58 kg CO_2e/MWh at zero wind penetration. Although the cost of the CAN mix is lower than the VI mix, emissions are higher at 200 kg CO_2e/MWh at zero wind penetration. Both regions have roughly the same amount of hydro capacity (10% less for CAN), but the CAN mix has carbon intensive coal capacity that is met with low carbon natural gas capacity in the VI mix. NWPP mix also has a significant portion of hydro (43%), but the remainder is met with mostly coal and natural gas, yielding emissions of 250 kg CO_2e/MWh at zero wind penetration. These three mixtures (VI, CAN and NWPP) have a significant amount of hydro generation, which yields an operating emissions level of roughly one third of the level of the coal dominated mixtures of US and MAIN, with zero wind emissions of 700 and 725 kg CO_2e/MWh, respectively.

The reduction in system operating emissions can be seen in Figure 25, but the difference in emissions compared to zero wind penetration is better illustrated by plotting the incremental emissions for each mixture (Figure 26). The incremental emissions for a specific mixture refer to the level of system emissions for a certain wind penetration, minus the emissions at zero wind penetration for that mixture.

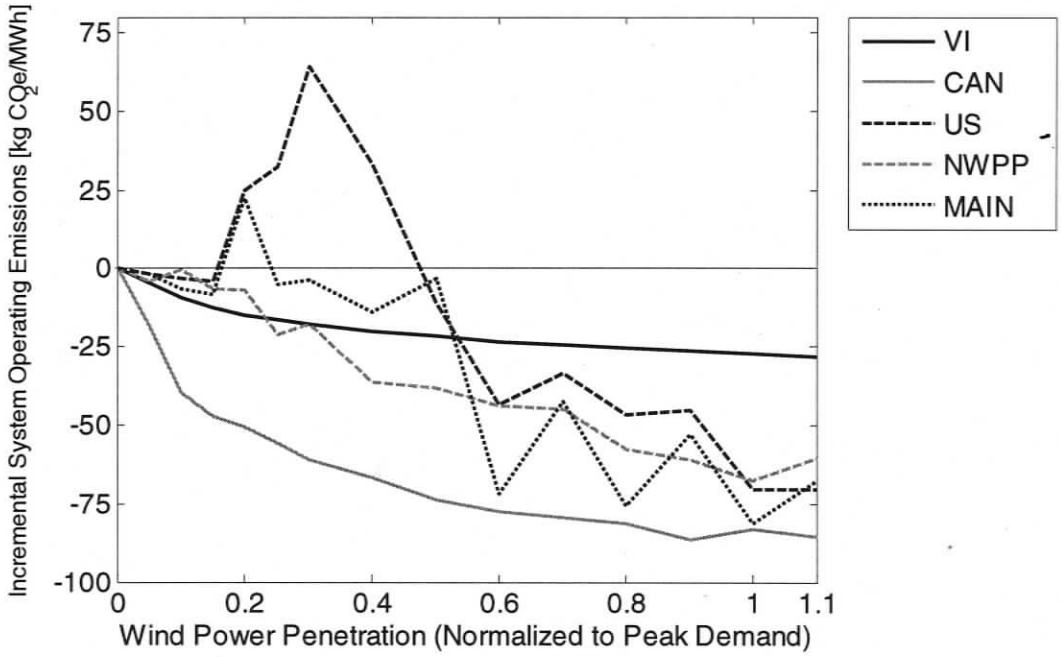

Figure 26. Incremental system operating emissions (compared to zero wind emissions) for the five mixtures.

For the VI mixture, Figure 26 shows a smooth reduction in emissions for the range of wind penetrations. The reduction in emissions for the VI mix is the lowest at full penetration, with a decline of 25 kg CO_2e/MWh; only a small reduction can occur in an already low emission mixture. The CAN mixture exhibits emission reductions for all

penetrations, with a reduction of 80 kg CO_2e/MWh at full wind penetration. The CAN mixture shows the largest emission reductions over the range of penetration because of the mixture's low percentage of natural gas and petroleum capacity and moderate amount of carbon intensive coal capacity. As wind generation grows for the CAN mix, it first replaces the small amount of expensive petroleum and natural gas capacity (9%), then replaces the next expensive source, which is coal capacity (12%). The initial reduction of carbon emitting sources and the large capacity of fast ramping hydro allows the CAN mix to reduce emissions to a large extent, without requiring large amounts of excess power from highly ramp constrained capacity.

Emissions for the US and MAIN mixtures initially increase for penetrations up to 50%, then decline by 75 kg CO_2e/MWh by the full range of wind penetration. These incremental emissions trends for US and MAIN mixtures are distinctly different from the other mixtures, which is due to the large amount of coal capacity in each (over 1000 MW). To explain these trends, the operating levels of the various generators in the US mixture will be examined. Average capacity factors for the several generators as a function of increasing wind penetration are provided in Figure 27 - six trends for the six individual generators and a seventh trend for the combined average capacity factor for the two nuclear facilities. The legend in Figure 27 indicates which trend line corresponds with each generator, and the network bus at which that generator is located.

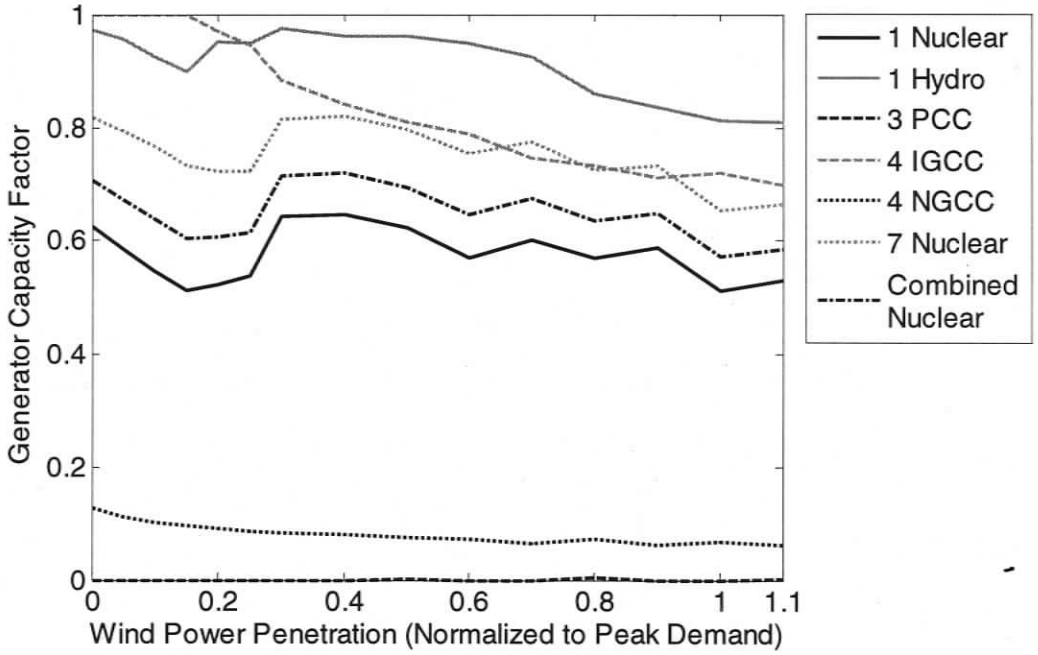

Figure 27. Average capacity factor as a function of increasing wind penetration for the various generators in the US mixture.

For the US mixture, emissions are primarily due to the coal facility, with the other emitters being the natural gas (NGCC) and petroleum generators (PCC). The petrol facility produces a negligible amount of carbon, and the natural gas facility produces less than 2% of the carbon produced from the coal facility. Thus the operating trend of the coal facility alone can be used to explain the initial increase in system emissions as wind penetration grows. In Figure 27, the average capacity factor for the coal generator drops from 100% to 70% for the range of wind penetrations. If the coal facility actually operated at the same average capacity factor for every hour in the entire two week period, then the emissions trend should continually rise for the range of wind penetrations due to

the continually falling capacity factor[4]. This is not the case, however; the coal facility does not operate near the same average capacity factor for the two week period. The coal generator either spends time at full capacity, or time at low capacity, and this behaviour is disguised by the average capacity factor. This can be shown well using generation duration curves for the coal generator. The duration curve sorts the level of generation from high to low over the 336 hours of operation. This sorting allows the visualization of how long a generator spends at each capacity level. Duration curves for the coal generation level are shown for various wind penetrations in Figure 28.

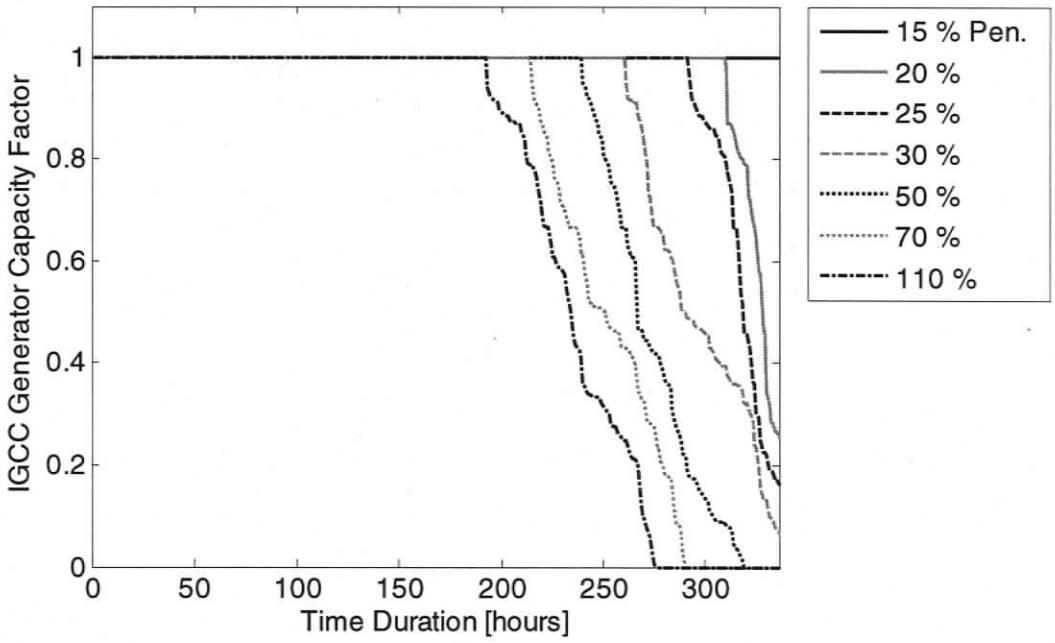

Figure 28. Generation duration curves for the coal facility (US mix) for various wind penetrations.

[4] If the capacity factor of a generator is continually falling, then the efficiency of the generator will fall as well. This reduction in efficiency leads to increased carbon emission intensity.

For wind penetrations up to and including 15%, the coal generator is never forced away from full capacity by wind intermittency, and the duration curves are simply straight lines at a capacity value of one. For these penetrations, the coal facility generates a steady amount of emissions, and the incremental emissions trend remains near zero (Figure 26). For wind penetrations between 15 and 40%, the coal capacity is reduced for a small number of periods, and emissions increase during these periods because coal is running at a lower efficiency. These times of low efficiency can be seen as the high slope portion at the end of the duration curve, which only consumes 20% of the duration at most (this 20% does not include times of zero generation). For wind penetrations above 40%, the number of periods that coal is reduced from 100% capacity and yet above zero output remains the same, and only periods of zero generation are appended at the end of the duration curve. Thus the increase in emissions due to low efficiency generation ceases to grow, times of zero output begin to replace the times when coal is at full capacity, and total emissions over the full period begin to decline. As penetration grows to 110%, more periods of zero generation replace times of 100% capacity, and emissions fall by 75 kg CO_2e/MWh compared to emissions at zero wind penetration.

These periods of reduced and zero coal generation are due to periods when wind generation peaks, forcing the coal generator to reduce output for an optimal cost solution. The solution attempts to reduce coal capacity quickly, but it's restricted to reduce by a maximum of one third of its capacity every hour due to the ramp rate restriction. For these periods, the optimal cost solution prefers coal at zero when wind spikes, but coal is unable to drop quickly, and increased emissions are associated with times when the capacity is between 0% and 100%. The same effect occurs when the wind power drops

quickly, and the optimal solution would like to bring coal up to 100% capacity quickly from zero. The ramp restriction is again in place, and there again exists periods of increased emissions and cost as the generator ramps up.

Plotting the coal emissions for the times at 100% capacity and for times at less than 100% capacity can help explain the incremental emissions trend further; these trends are shown in Figure 29.

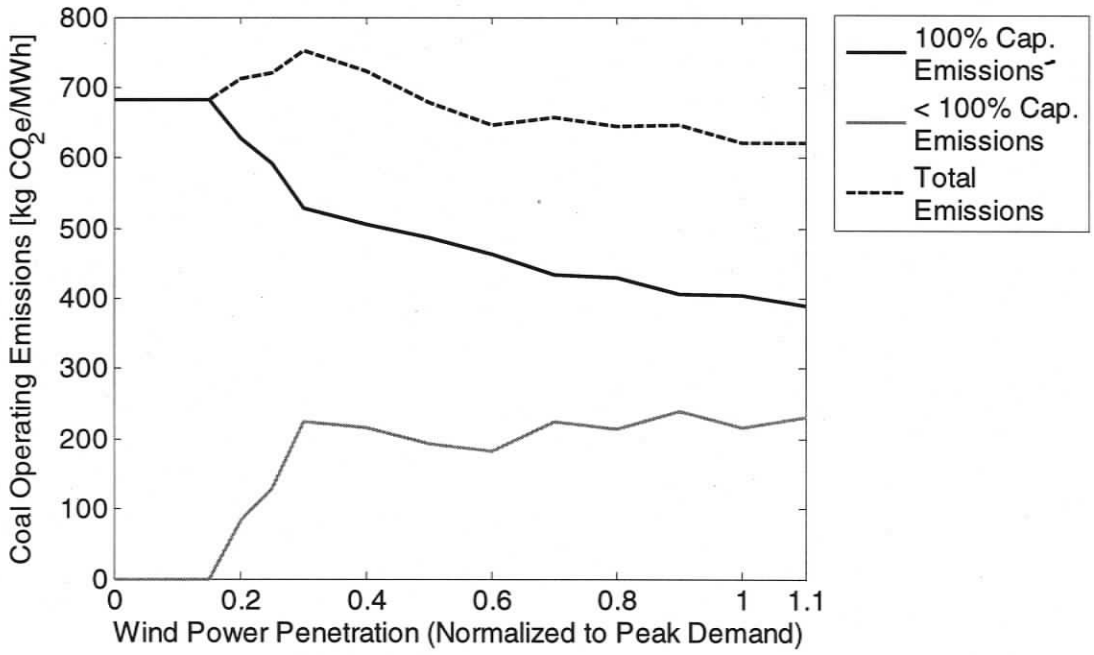

Figure 29. Carbon emissions produced by the coal facility (US mix), separated into emissions at full capacity and emissions at reduced capacity.

As wind penetration grows from 15 to 110%, the amount of emissions produced when the coal facility is at 100% capacity continually declines. This occurs because of the declining number of periods that the facility is operated at full capacity. As wind penetration grows from 15 to 30%, the amount of emissions produced when the coal

facility is below 100% increases due to operation at a lower efficiency. At wind penetrations above 30%, times of zero capacity instead of times of low capacity replace times at full capacity, and the emissions for "< 100%" trend remain steady near 225 kg CO_2e/MWh. These steady and unsteady trends sum together to give the overall emissions trend for the coal facility: emissions increase up to 50% wind penetration and then decline for larger wind penetrations.

These results show that wind integration into a mixture with a large amount of coal capacity can cause an increase in system operating emissions. A large coal facility will exhibit a large increase in operating cost and emissions when operated away from full capacity. Thus the optimal cost solution attempts to keep the coal facility at full capacity until times of large wind input, when the optimal solution does not require the coal generator to meet demand and would rather have it at zero capacity. The ramp restriction on the generator forces some part load operation during the times the solution switches the generator on and off and emissions from the facility distinctly increase. At larger wind penetrations there exists more periods when the coal generator remains at zero capacity between being shut off and on. Times at zero capacity eventually offset the time spent at part load and a reduction in emissions is observed.

7.4.3 Economic Dispatch between Coal and Nuclear

It can be seen in some capacity factor trends (US, MAIN, NWPP) that coal capacity is used more frequently than cheaper nuclear capacity. This is not an intuitive result due as the objective is to minimize cost, and nuclear always has a lower cost than coal, irrespective of their part loads. The average capacity factors for the generators in the

US mix was shown in Figure 27, and the average capacity factor trends for the MAIN and NWPP mixtures are shown in Figures 30 and 31, respectively.

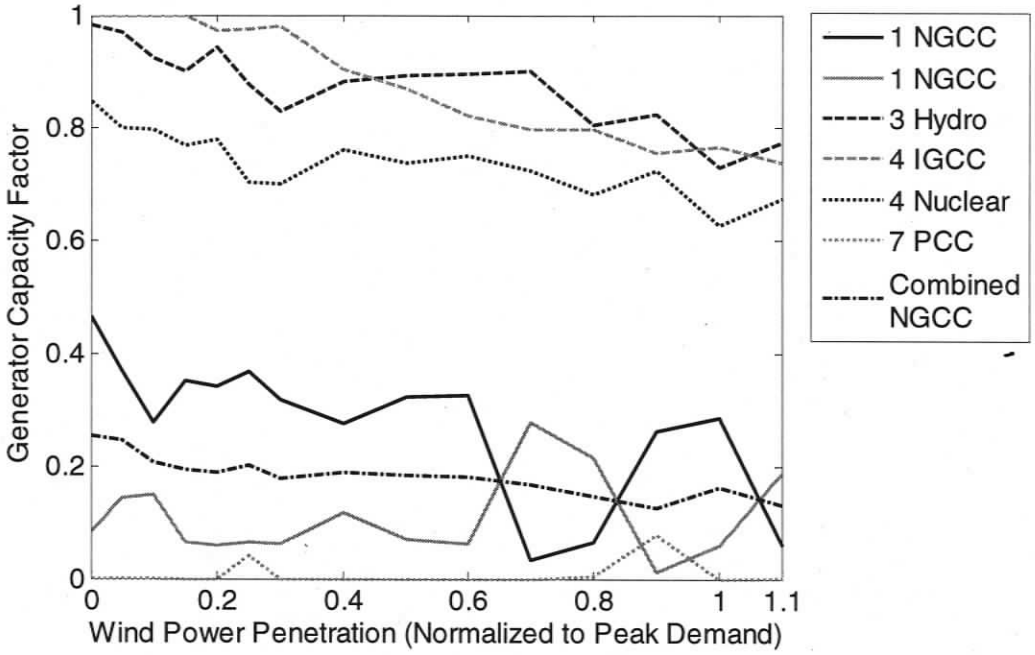

Figure 30. Average capacity factor as a function of increasing wind penetration for the various generators in the MAIN mixture.

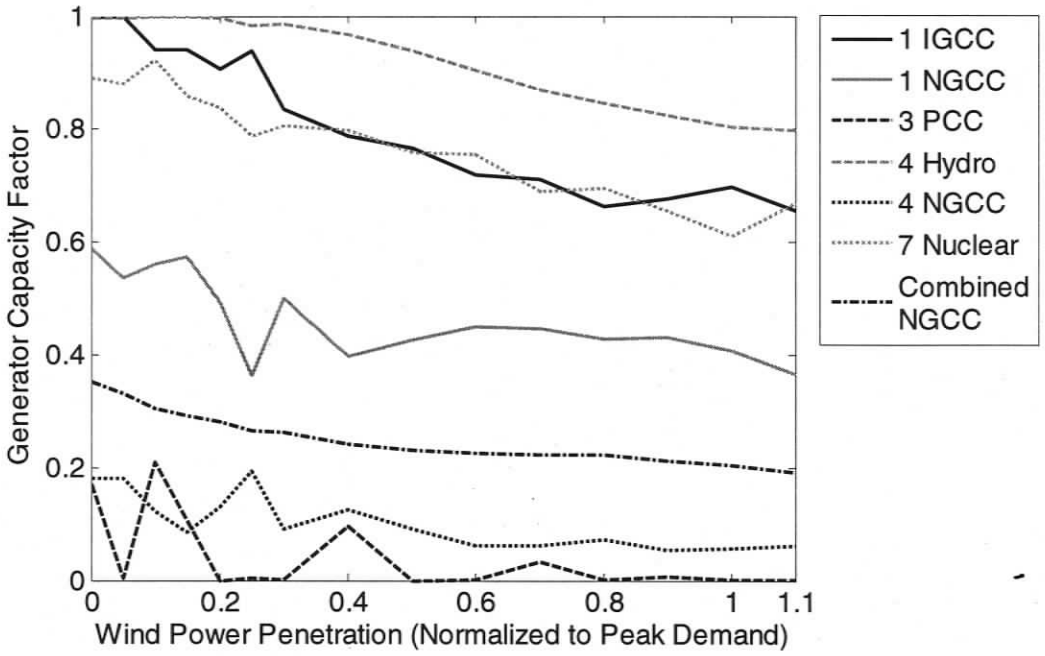

Figure 31. Average capacity factor as a function of increasing wind penetration for the various generators in the NWPP mixture.

When a coal generator and a nuclear generator are directly contending to meet a common demand, it is more economic for total cost to keep the capacity factor of the coal facility either below 36%, or at 100%. This can be shown visually by calculating the total cost of one coal and one nuclear generator meeting a constant load over a range of coal capacity factors. Figure 32 shows the cost of one IGCC generator and one nuclear generator (both sized at 100 MW capacity) meeting a 100 MW load for a single hour. The horizontal axis of Figure 32 plots the capacity factor of the IGCC generator; when the capacity factor of the coal generator is reduced from 100%, the capacity factor of the nuclear facility must increase to satisfy the unmet demand. The vertical axis of Figure 32 plots the total cost of meeting the demand over one hour divided by the generating

capacity of the coal facility (100 MW). Appendix B discusses the creation of Figure 32, illustrating the equations and process leading to the plot.

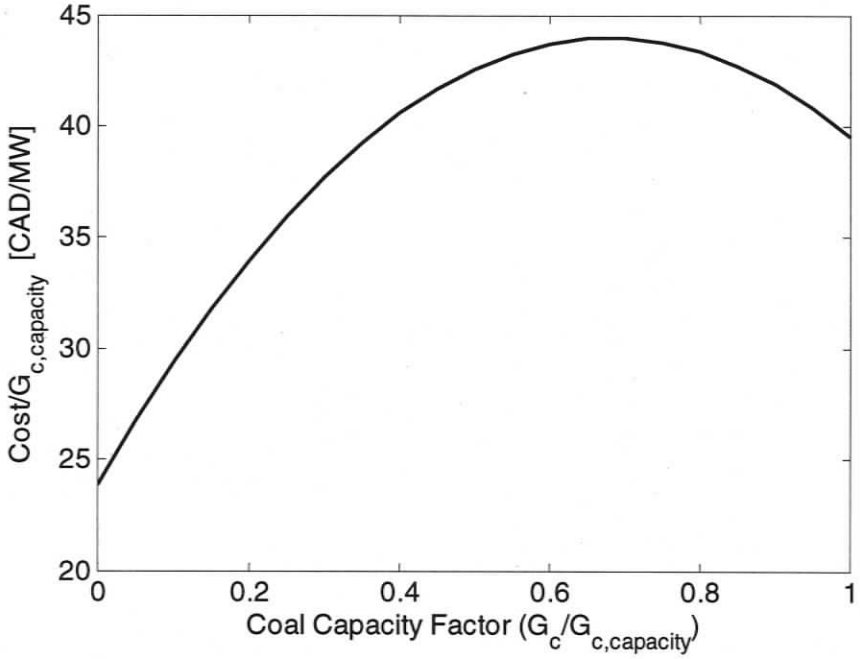

Figure 32. The cost of one coal and one nuclear generator meeting a 100 MW load for a single hour.

It can be seen in Figure 32 that a certain cost is associated with meeting the load at 100% coal capacity, 40 CAD/MW. If the capacity factor of the coal generator is reduced from 100%, then the total cost increases, and an economic penalty is incurred. Total cost exhibits an increase at reduced coal capacity factors until a factor of 36%, but moving below 36% results in an economic benefit.

This explains why coal is used at a higher capacity factor for the US, MAIN and NWPP mixtures (Figures 27, 30 and 31). Coal generation is forced above a capacity factor of 36% to meet demand, and the solution keeps the coal facility generating at full capacity to minimize system cost; until times when high wind power allows the reduction

of coal capacity to below 36%. Due to the high generating level of the coal facilities, the nuclear facilities are not fully required to meet demand and their average capacity factor is lower than that of coal. It should be noted that this switch in economic benefit/penalty at 36% coal capacity factor is entirely dependant on the cost coefficients used for these two generation technologies, and would change if more accurate efficiency profiles were available.

The average capacity factors for the CAN mixture are shown in Figure 33, where the reversal of the coal-nuclear tradeoff can be seen. Coal generation is not required above a capacity factor of 36% to meet demand, thus it is kept at a low operating level to yield minimum system cost. Nuclear capacity is used to meet a large portion of demand instead of coal, and its average capacity factor remains above that of coal for the range of wind penetration.

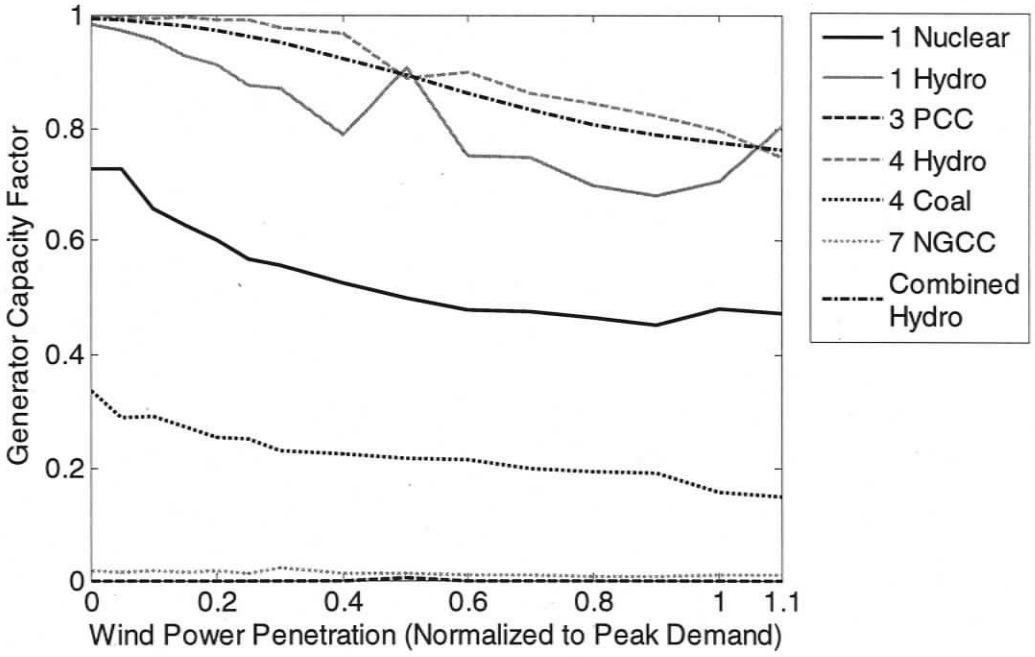

Figure 33. Average capacity factor as a function of increasing wind penetration for the various generators in the CAN mixture.

Nuclear and wind would have the same type of cost profiles if an O&M cost was associated with wind; they would both be below the cost of coal and have low variance. Thus the dispatch tradeoff between coal and nuclear could occur between coal and wind, if wind was no longer considered "must run" and the solver had a choice to use wind power or not. For the results presented in this thesis, wind power must be used by the network to meet demand when it is available. If there was a choice associated with the use of wind power, and wind was integrating into a system with large amounts of coal capacity, then an optimal cost solution may not choose to use available wind power in order to keep coal at full capacity.

8. Discussion and Conclusions

In this thesis, an optimal power flow model was formulated that considered the interaction between existing and new generation technologies under the constraint of an existing transmission network. The optimization problem was formulated as a quadratic program with linear constraints, solved over two-week periods using an hourly resolution and minimizing generation cost. The network model approximates the actual transmission network on Vancouver Island, British Columbia. Wind generation was introduced into the modeled network, coexisting with various generation mixtures of natural gas thermal plants, petroleum thermal plants, coal thermal plants, nuclear plants and large-scale hydroelectric facilities. This study provided results regarding network constraints when introducing wind power into a system, and the induced effect that wind had on the existing generators. The study also examined system operating cost when wind integrated with the existing Vancouver Island electricity system, with and without the consideration of a capital cost for the wind farm. System operating cost was also examined when wind integrated with various other mixtures, including four other pertinent regions. Wind's effect on system carbon dioxide emissions was analyzed for each mixture, and an interesting trend involving coal fed generation was discussed. Results for this study concluded with discussing a phenomenon that occurs when economically dispatching coal and nuclear facilities to meet a common load, and how this situation could occur between coal and other technologies with the same cost characteristics as a nuclear facility.

8.1 Network Constraints and Wind Induced Effects on Existing Generators

Results show that the wind farm capacity factor is limited due to transmission capacity constraints, and that the energetic capacity factor of the wind farm must decline if penetration is to exceed 10% into the Vancouver Island network. If power penetration is to exceed 10% without a decline in capacity factor, transmission capacity to the Northern region of Vancouver Island must be increased. When wind power penetration exceeds 60% during peak demand periods, wind generation will exceed demand in some non-peak periods and power must be exported.

Using load duration curves, base-load generating potential falls with increased wind penetration, with base load eliminated entirely at 60% penetration in the case of winter demand. As wind penetration increases, the generators in the network experience a drop in their capacity factor, leading to more frequent operation at part load and thereby a reduction in average operating efficiency. The fall in average efficiency leads to an increase in average operating cost and emissions for the existing generators.

8.2 Operating Cost on Vancouver Island

Results also show that system costs begin to decline rapidly as small amounts of zero-cost wind enter the network. As wind penetration grows, the average costs of the existing generators increase, and the benefit of introducing zero-cost wind into the system declines. For the Vancouver Island generation mix, system operating costs fall for the full range of wind penetration up to 110%. However, when the amortized capital cost of the wind installation was included, system costs declined until 15% penetration, but then

grew to one and a half times the zero wind cost, resulting in a net negative benefit for wind penetration beyond 30% (assuming no network constraints).

The Vancouver Island network is dominated by hydroelectric power (70%), resulting in an inexpensive system generation cost at zero wind penetration – 1.25 Canadian cents per kilowatt-hour. If wind was to enter a thermal-dominated network, system generation costs would be substantially larger, and the effect of incorporating the capital cost of the wind farm would not be such an overriding component of the total increase in system costs.

8.3 Operating Cost and Network Export for Various Generation Mixtures

Five different generation mixtures were examined, showing a wide range of system operating cost due to varying technology capacities. The zero wind cost of the CAN, VI, NWPP, US, and MAIN mixtures were 10, 13, 24, 35 and 39 CAD/MWh, respectively, with almost a four fold variation between the cheapest and most expensive mixture. When the incremental operating cost for the various mixtures was examined, wind provides the largest cost reduction for thermal dominated mixtures with lower amounts of ramp constrained capacity. The three thermal dominated mixtures (US, MAIN and NWPP) all show large cost reductions at the full range of wind penetration; however, the two highly ramp constrained mixtures (US and MAIN) show less cost reduction for moderate penetration due to the cost of their excess generation. When neglecting wind farm capital cost, the cost reductions for the CAN, VI, NWPP, US and MAIN mixtures at 110% penetration were 4, 6, 8.5, 9 and 10 CAD/MWh, respectively.

When an amortized capital cost of the wind farm was included, the range of penetration that each mixture exhibited a reduction in cost was altered. The VI mix fell by a maximum of 1 CAD/MWh at a penetration of 15%, but then grew and caused system cost to increase with penetrations above 30%. In the NWPP mix cost fell by a maximum of 1.5 CAD/MWh at a penetration of 30%, but then costs grew and caused system cost to increase with penetrations above 70%. The MAIN mix varied near a cost reduction of 0.5 CAD/MWh for up to 80% penetration, but then system cost increased for higher penetrations. Both the CAN and US mixtures resulted in cost increases for the entire range of penetration, except for a negligible decrease for up to 10% penetration for the CAN mix, and a negligible decrease at 60% penetration for the US mix.

High ramp constrained mixtures export power from the network for the range of wind penetration examined due to the inability of some generators to reduce output at times of large decreases in wind generation. The three mixtures with large hydroelectric capacities (VI, CAN and NWPP) also export power for penetrations above 60%, and results indicate that this export was due to wind power exceeding demand, and not due to ramp restrictions on generators.

8.4 Operating Emissions for Various Generation Mixtures

The operating emissions from each mixture were also examined, showing a wide range of values due to the differing carbon intensities of various fuels. The zero wind system emission levels of the VI, CAN, NWPP, US and MAIN mixtures were 55, 200, 250, 700 and 725 kg CO_2e/MWh, respectively. Incremental emission trends show a comparison of the reduction in system emissions between the various mixtures, with

wind reducing emissions the most in the CAN mix due to low ramp constrained capacity and the early replacement of natural gas and coal capacities. The smallest emissions decline due to wind penetration was observed for the VI mix, which already had low emissions with zero wind penetration, which resulted in the inability of wind capacity to replace emission intensive capacity. At 110% wind penetration, the VI, NWPP, US, MAIN,\ and CAN mixtures exhibited a decline in system emissions of 25, 65, 75, 75 and 80 kg CO_2e/MWh, respectively. Emissions increase in the US and MAIN mixtures, but begin to decrease at a wind penetration of 50%. These two emission profiles are primarily due to the coal facilities which that up the majority of the capacity in the US and MAIN mixtures. This trend showing the increase then decrease in emissions can be explained using the operating trend of the coal facility for the US mix. The optimal cost solution lets the coal generator run at full capacity, until times of large wind input into the network, when the solution prefers to run the coal generator at zero capacity. The solver did not prefer to have the coal generator operating at part load due to the high cost of such operation, but part load operation was forced to occur due to the ramping restrictions of the facility. The forced times at part load for the coal generator forced an increase in emissions. As wind penetration grew, the times of high wind speed did not change; thus, the times when the solution desired zero coal did not change and the emissions produced during part load operation remained steady. Times of zero coal capacity began to replace times of full coal capacity, and emissions decline for large wind penetrations.

8.5 Economic Coal Dispatching

Coal capacity replaces lower cost nuclear capacity for some generation mixtures. Maintaining coal generation at full capacity and nuclear at part load operation yields a lower system cost compared to scenarios of full nuclear capacity and coal at part load operation. This is the case if coal generation is forced above 36% capacity to meet demand, but not if coal capacity is not required above 36% capacity to meet demand. This economic dispatching decision can occur between coal and wind, but only if the solver has the option to use or not use available wind power when desired and a small cost is associated with wind power. If a coal facility runs at a high capacity factor, and low cost wind became available, the solution might not choose to use the wind power, due to the increase in cost of reducing the operating efficiency of the coal facility.

8.6 Generation Mixture Attributes Leading to Beneficial Wind Integration

Wind penetration may seem favorable for mixtures that have a high capacity of fast ramping generators, such as hydroelectric generators. However, the results indicate that wind makes the largest cost reductions in thermal dominated mixtures, as long as the thermal facilities are not highly ramp constrained. Forced part load operation due to ramp restrictions occurs in some thermal dominated mixtures, depleting the cost reduction that wind imposes on the system. Introducing wind generation should lower system emissions, as wind replaces carbon emitting sources, more noticeably in thermal dominated mixtures. This is the case of the thermal dominated mixtures that are not heavily ramp constrained; but it is not the case for highly ramp restricted mixtures, which

show increases in system operating emissions for moderate penetrations, lowering the benefit of installing the zero carbon, zero cost wind capacity.

9. Recommendations

Future development of the model will need to include storage at buses, such that non-dispatchable power can be stored from one time period to the next. Storage facilities will include rate constraints to limit the amount of power a system can absorb or produce during a single time step, with the inclusion of round-trip efficiencies and maximum storable energy. Minimum cut-off limits will also be included for dispatchable generators, so that a facility will stop generating power when its part-load output falls below a specified lower limit. Installation of additional generation or transmission capacity can be made a decision variable in the model, so that associated capital costs will be included. This enables one to analyze the benefits and drawbacks of installing additional transmission capacity or possibly a fast ramping thermal facility. These modifications are also important because they enable one to measure the costs of reducing CO_2 emissions, an important policy consideration.

Future additions will also include an operating and maintenance cost for wind power, such that some cost can be applied to the electricity source. As indicated in this thesis, including a capital cost for the wind farm resulted in drastic alterations to system cost, and including O&M costs in the analysis would apply some cost to wind that would fall between zero cost and the capital cost.

Bibliography

1. Department of Energy/Energy Information Administration, International energy outlook 2005.

2. Asif M, Muneer T, Energy supply, its demand and security issues for developed and emerging economies. Renewable & Sustainable Energy Reviews 2005; Article in Press.

3. Kennedy S, Wind power planning: assessing long-term costs and benefits, Energy Policy 2005; 33: 1661-1675.

4. J.A. Momoh, M.E. El-Hawary, R. Adapa, A review of selected optimal power flow literature to 1993 part I: Nonlinear and quadratic programming approaches. IEEE Transactions on Power Systems 1999; Vol. 14 No. 1: 96-104.

5. DeCarolis J, Keith D, The economics of large-scale wind power in a carbon constrained world. Energy Policy 2006; 34: 395 – 410.

6. S. Jebaraj, S. Iniyan, A review of energy models. Renewable and Sustainable Energy Reveiws 2006; 10: 281-311.

7. J. Carpentier, Contribution a. 'l'etude du dispatching economique. Bulletin de la societe francaise des electricians 1962; 3: 431-447.

8. El Abiad A, Jaimes F, A method for optimum scheduling of power and voltage magnitude. IEEE Transactions on Power Apparatus and Systems 1969; PAS-88 No.4: 413-422.

9. Dommel H, Tinney W, Optimal power flow solutions. IEEE Transactions on Power Apparatus and Systems 1968; PAS-87: 1866-1876.

10. Sasson A, Combined use of the parallel and Fletcher-Powell non-linear programming methods for optimal load flows. IEEE Transactions on Power Apparatus and Systems 1969; PAS-88 No.10: 1530-1537.

11. Barcelo W, Lemmon W, Koen H, Optimization of the real-time dispatch with constraints for secure operation of bulk power systems. IEEE Transactions on Power Apparatus and Systems 1977; PAS-96 No.3: 741-757.

12. Talukdar S, Giras T, Kalyan V, Decompositions for optimal power flows. IEEE Transactions on Power Apparatus and Systems 1983; PAS-102 No.12: 3877-3884.

13. F.J. Heredia, N. Nabona, Optimum short-term hydrothermal scheduling with spinning reserve though network flows. IEEE Transactions on Power Systems; Vol. 10 No. 3: 1642-1651.

14. T. Yalcinoz, O. Koksoy, A multiobjective optimization method to environmental economic dispatch. Electrical Power and Energy Systems 2007; 29: 42-50.

15. S. Lee, Economic location of industrial fuel cell in a power system using cost sensitivity derived by normal power flow. Journal of Power Sources 2006; 157: 828-831.

16. C. Chen, Non-convex economic dispatch: a direct search approach. Energy Conversion and Management 2007; 48: 219-225.

17. J. Soderman, F. Pettersson, Structural and operational optimization of distributed energy systems. Applied Thermal Engineering 2006; 26: 1400-1408.

18. J.B. Greenblatt, S. Succar, D.C. Denkenberger, R.H. Williams, R.H. Socolow, Baseload wind energy: modeling the competition between gas turbines and compressed air energy storage for supplemental generation. Energy Policy; Article in Press.

19. P. Denholm, G.L. Kulcinski, T. Holloway, Emissions and energy efficiciency assessment of baseload wind energy systems. Environmental Science and Technology 2005; 39: 1903-1911.

20. J.K. Kaldellis, K.A. Kavadias, Optimal wind-hydro solution for Aegean Sea islands' electricity-demand fulfillment. Applied Energy 2001; 70: 333-354.

21. M.A. Elhadidy, S.M. Shaahid, Decentralized/stand-alone hybrid wind-diesel power systems to meet residential loads of hot coastal regions. Energy Conversion and Management 2005; 46: 2501-2513.

22. D. Weisser, R.S. Garcia, Instantaneous wind energy penetration in isolated electricity grids: concepts and review. Renewable Energy 2005; 30:1299-1308.

23. Brooke A, Kendrick D, et al, GAMS. A user's guide 2005, Washington, DC, GAMS Development Corporation.

24. Auer P, Advances in energy systems and technology 1978. Vol. 1. New York, Academic Press.

25. Institute for Energy Technology, HYDROGEMS, P.O. Box 40, NO-2027, Kjeller, Norway.

26. Enercon, E70 technical data sheet, 2005. http://www.enercon.de/en/_home.htm

27. BC Hydro, private communication, 2003.

28. Canadian Electricity Association, Power generation in Canada, 2006.

29. Department of Energy/Energy Information Administration, Existing capacity by energy source, 2005.

30. Department of Energy/Energy Information Administration, Existing nameplate and net summer capacity by energy source and producer type (EIA-860), 2004.

31. Department of Energy/Energy Information Administration, Natural gas weekly update, October 1st, 2006. http://tonto.eia.doe.gov/oog/info/ngw/ngupdate.asp

32. Department of Energy/Energy Information Administration, Coal news and markets, October 1st, 2006.
http://www.eia.doe.gov/cneaf/coal/page/coalnews/coalmar.html#spot

33. Department of Energy/Energy Information Administration, Spot prices, conventional regular gasoline, October 1st, 2006.
http://tonto.eia.doe.gov/dnav/pet/pet_pri_spt_s1_d.htm

34. Department of Energy/Energy Information Administration, Assumptions for the annual energy outlook 2006 with projections to 2030, 2006.

35. Kim T S, Comparative analysis on the part load performance of combined cycle plants considering design performance and power control strategy, Energy 2004; 29: 71-85.

36. Organization for Economic Co-operation and Development/International Energy Agency, Nuclear power in the OECD, 2001.

37. Ministry of Environment, Province of British Columbia, Annual water license rental rates associated with power production, February 2006.
http://www.env.gov.bc.ca/wsd/water_rights/water_rental_rates/cabinet/new_rent_structure_waterpower.pdf

38. RETScreen International, Natural Resources Canada, Francis turbine efficiency, 2004. http://www.retscreen.net/

39. Idaho National Engineering and Environmental Laboratory, Estimation of economic parameters of U.S. hydropower resources, June 2003.

40. BC Hydro, Wind Data Release #2, August 2004. http://www.bchydro.com/environment/greenpower/greenpower1764.html

Appendix A – Calculation of Cost Parameters

A.1 Calculation of Fuel Cost Coefficients for a Natural Gas Combined Cycle Facility

This section demonstrates the process associated with calculating the cost coefficients $A_{d,c}$ and $B_{d,c}$ that approximate the variable fuel cost for a natural gas combined cycle facility.

The process begins with the thermal efficiency of the generator as a function of its part load, ranging from zero to one. This efficiency curve was obtained as several data points from [35], and is plotted in Figure A1, along with a linear trend line fitted to the data points.

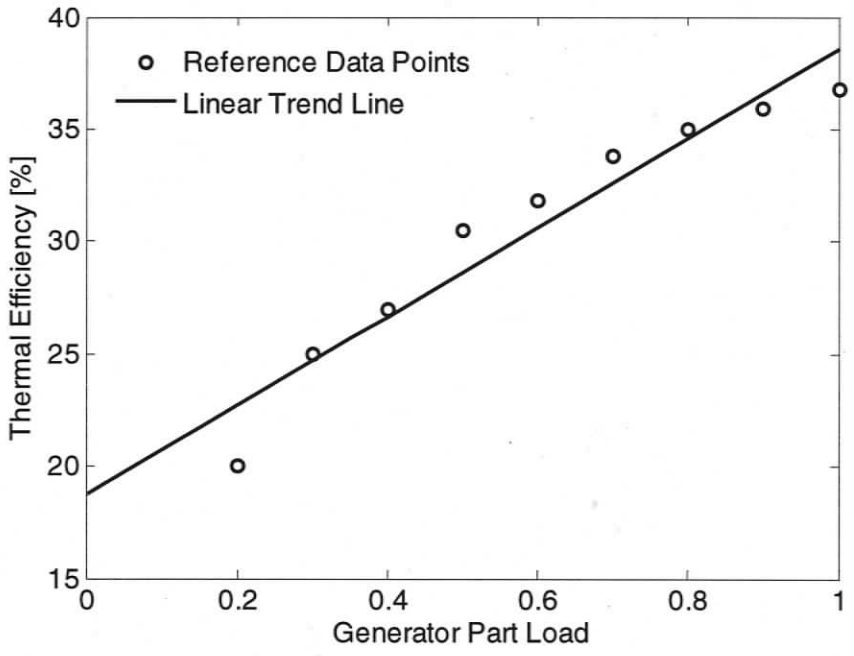

Figure A1. Data points and linear trend line for the thermal efficiency of a natural gas combined cycle facility.

The peak efficiency of the linear approximation is 38.6%; however, data from [34] indicate that current natural gas combined cycle technology can achieve peak efficiencies of 47.4%. The efficiency approximation is scaled to yield the peak efficiency provided by [34]. The scaling equation used is listed below as Equation (A1):

$$\eta_{scaled} = \frac{47.4}{38.6}\eta_{original} \tag{A1}$$

where η_{scaled} is the scaled efficiency with a peak of 47.4%, and $\eta_{original}$ is un-scaled efficiency with a peak of 38.6%. The scaled and original efficiency trends are plotted together in Figure A2.

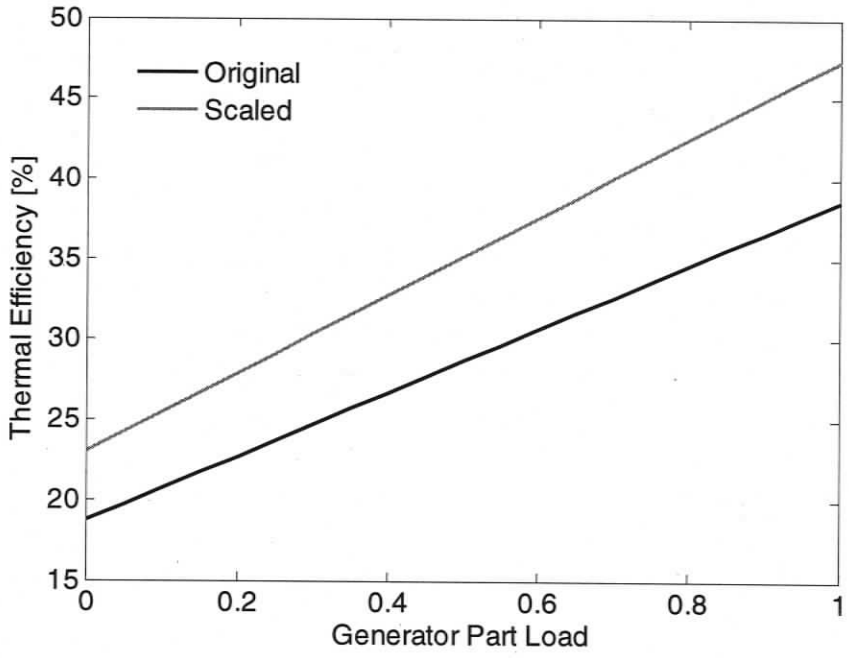

Figure A2. The original combined cycle efficiency trend and a scaled trend corresponding to current technology.

The cost coefficients $A_{d,c}$ and $B_{d,c}$ represent the fuel cost to produce one MWh of electricity. When calculating the required input energy to produce one MWh of electricity, the one MWh output remains constant and thermal efficiency is varied to yield input energy at any loading. Equation (A2) illustrates how a variable efficiency is used to calculate required input energy to produce a single MWh of electricity:

$$Energy_{Input} = \frac{Energy_{Output}}{\eta} \tag{A2}$$

where $Energy_{Input}$ is the quantity of fuel [MWh] required to produce the $Energy_{Output}$ of one MWh at a given thermal efficiency η. A fuel cost having units of \$/MWh must be applied to the input energy to obtain a cost of CAD per generated MWh of electricity.

A natural gas spot price of 8 USD/MMBtu is assumed [31] equivalent to a natural gas cost of 31 CAD/MWh. This cost is then applied to the amount of fuel energy required to produce one MWh of electricity, and a cost per produced MWh of electricity is obtained. Thus, the efficiency curve in Figure A2 is converted to a fuel cost as a function of part load. The resulting curve is plotted in Figure A3, along with a linear trend line fitted to the data points.

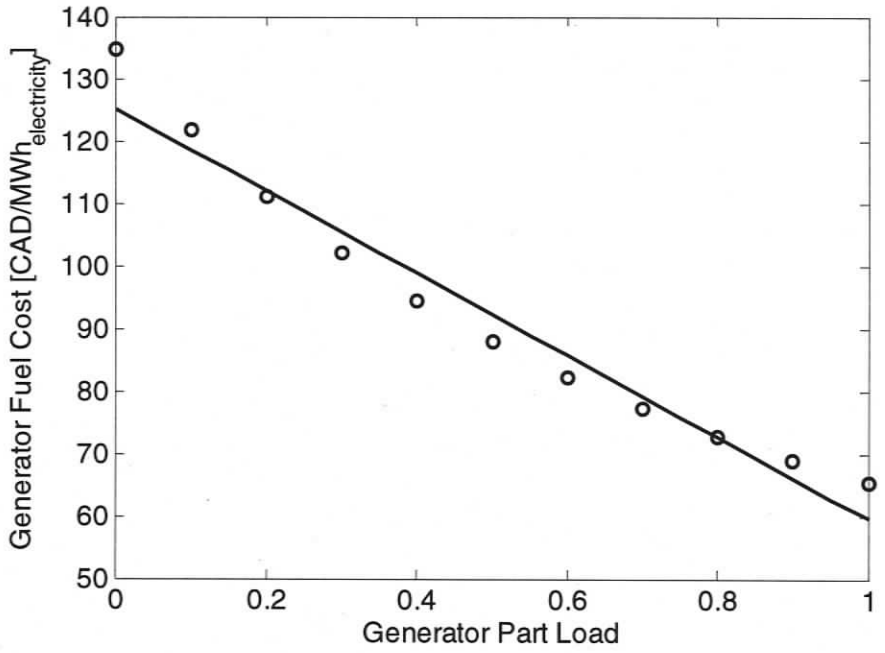

Figure A3. Data points showing the fuel cost of operating a natural gas combined cycle facility with respect to its part load, and a linear trend line fitted to the data points.

The linear cost trend line in Figure A3 can be represented by a slope and a vertical axis intercept term, and these are the $A_{d,c}$ and $B_{d,c}$ coefficients, respectively, that describe the variable fuel cost for the generator. The slope of the linear trend line is -65.12 CAD/MWh, hence $A_{d,c}$ = -65.12 CAD/MWh. The vertical intercept of the linear trend line is 125.28 CAD/MWh, hence $B_{d,c}$ = 125.28 CAD/MWh.

A.2 Calculation of Fuel Cost Coefficients for a Hydroelectric Facility

This section demonstrates the process for determining the cost coefficients $A_{d,c}$ and $B_{d,c}$ that approximate the variable water cost for the BC average hydroelectric facility.

The process begins with the efficiency of the hydro turbine as a function of normalized flow rate, ranging from zero to one. Normalized flow rate refers to the actual flow rate moving through the turbine divided by the maximum flow rate (also assumed to be the design flow) that the turbine will experience. The efficiency data points shown in Figure A4 correspond to a Francis turbine with a design flow rate of 10 m^3/s and a head height of 100 m. Efficiency was calculated using equations provided by RETScreen [38] for a Francis turbine. A linear trend line is also plotted in Figure A4, but does not correspond to a minimum variance fit to the data points. The best fit trend line results in efficiencies greater than one for flow rates above 80%. Efficiencies above one are not attainable, so the peak of the linear trend was scaled down to correspond to the value at peak flow, while keeping the vertical intercept constant at 20% efficiency. All hydro facilities use the linear efficiency trend shown in Figure A4 to calculate water cost.

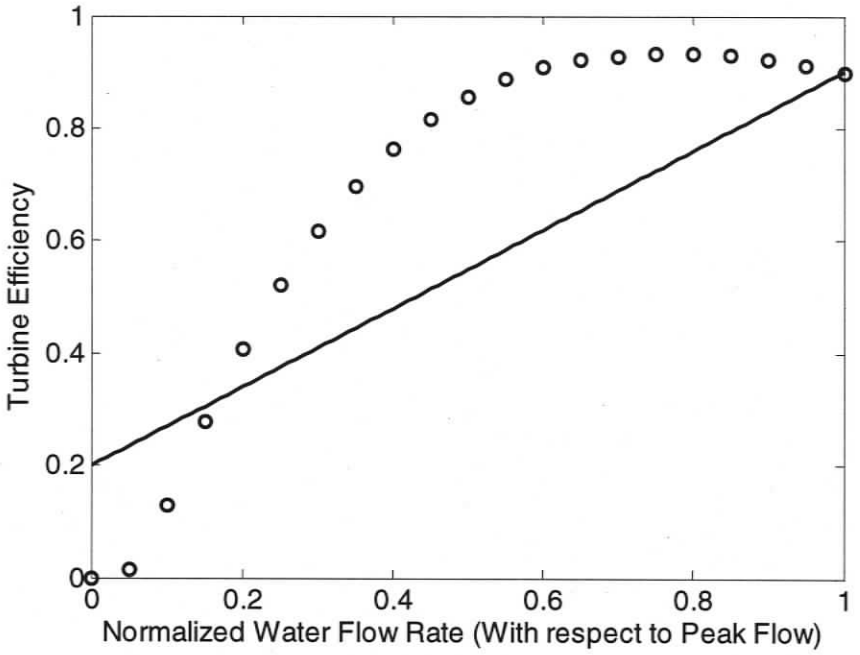

Figure A4. Data points and linear trend line for the turbine efficiency of a Francis turbine with respect to normalized water flow rate.

The cost of a specific hydro facility depends on the head, H, and the peak water flow rate at that facility, $\dot{Q}$. For the facility described in this section, the head is 160 m, and the peak flow is 637 m^3/s. This peak flow is large, and it should be noted that this flow corresponds to producing a peak power of 900 MW from the facility, a large capacity. As water flow increases from zero to one, actual water flow rate for the considered facility will grow linearly from zero to 637 m^3/s.

Power generation from the hydro facility is calculated using Equation (A3):

$$G = \frac{\rho \cdot g \cdot H_{head} \cdot \dot{Q} \cdot \eta}{1 \times 10^6} \tag{A3}$$

where G is the power generated in MW, ρ is the density of water in kg/m^3, g is the standard acceleration of gravity, H_{head} is the head height into the turbine in m, $\dot{Q}$ is the

flow rate through the turbine in m^3/s, η is the efficiency of the turbine (which is a function of flow rate), and the factor of a million converts power generation from W to MW.

Two costs have been applied to hydroelectric power generation for this thesis. There is a cost associated with generating energy, 1.086 CAD/MWh [37], and there is a cost associated with the volume of water used for generation, $6x10^{-6}$ CAD/m^3 [37]. The energy cost is applied to each MWh generated, and the volume cost is applied to each cubic meter of water used for generating power.

Power generation in MW is calculated over a range of flow rates, increasing from zero to the peak 637 m^3/s. For each flow rate (units of m^3/s), the cost of $6x10^{-6}$ CAD/m^3 is applied to the volume of water used, and then multiplied by a factor of 3600 seconds per hour to obtain a water cost over a period of an hour. This volume cost has units of CAD/h, and the equation for its calculation is:

$$Cost_{Volume}\left[\frac{CAD}{h}\right] = \dot{Q}\left[\frac{m^3}{s}\right]\cdot\left(6\times10^{-6}\left[\frac{CAD}{m^3}\right]\right)\cdot 3600\left[\frac{s}{h}\right] \tag{A4}$$

The cost shown in Equation (A4) is the water volume cost of generating G MW's over one hour. Generating one MW of power is the same as generating one MWh of energy over a period of an hour; thus, the units of G in MW are equivalent to units of MWh/h. The volume cost, converted to units of CAD/MWh can be obtained by dividing $Cost_{Volume}$ by G:

$$c_{hydro,volume}\left[\frac{CAD}{MWh}\right] = \frac{Cost_{Volume}\left[CAD/h\right]}{G\left[MWh/h\right]} \tag{A5}$$

The water volume portion of hydro cost, $c_{hydro,volume}$, is now obtained, in the proper units of CAD/MWh. The energy portion of hydro cost, $c_{hydro,energy}$ = 1.086 CAD/MWh, is already defined in the proper units and can simply be added to $c_{hydro,volume}$ to obtain the full hydro cost, c_{hydro}.

The water volume portion of cost is a function of efficiency, and thus it varies with respect to generator part load. The energy portion of cost is constant, and does not vary with respect to generator part load.

Total hydro cost with respect to normalized flow rate has now been formulated. When increasing the flow rate from zero to peak, the generated power also increases from zero to its peak. Power generation is normalized and deemed *generator part load*, and the cost of operating the facility (c_{hydro}) can be varied with respect to generator part load instead of normalized water flow rate. Figure A5 shows these data points, hydro generating cost with respect to its part load.

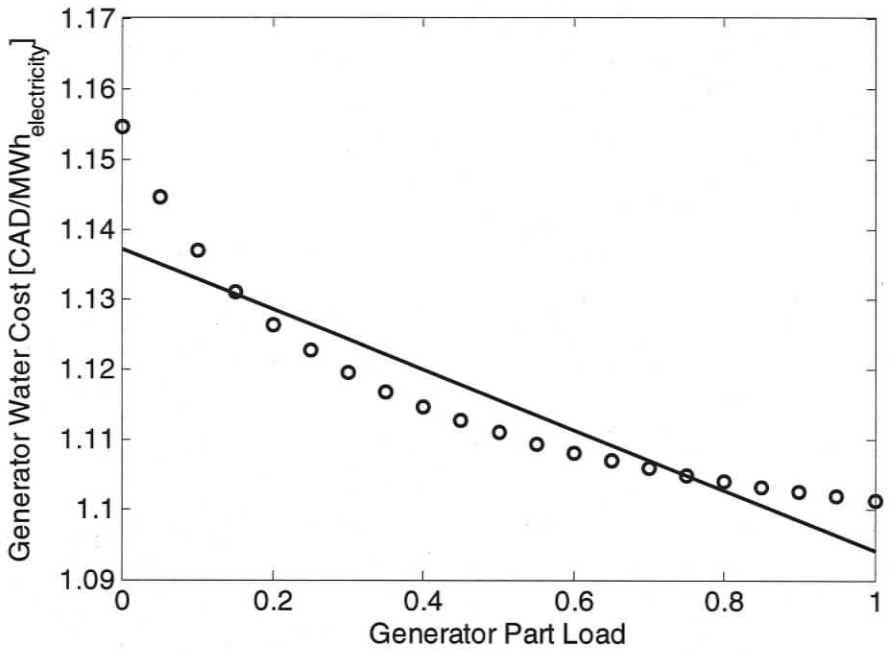

Figure A5. Data points showing the water cost of operating a hydroelectric facility with respect to its part load, and a linear trend line fitted to the data points.

Again, the linear cost trend is represented by a slope and a vertical axis intercept term, $A_{d,c}$ and $B_{d,c}$, respectively. The slope of the linear trend line is $A_{d,c}$ = -0.0432 CAD/MWh. The vertical intercept of the linear trend line is $B_{d,c}$ = 125.28 CAD/MWh.

Appendix B – Cost Calculation of One Coal and One Nuclear Generator

This section demonstrates the algebraic process leading to the plot shown in Figure 32 in Section 7.4.3. One coal generator and one nuclear generator are used to meet a common load, and calculating the total cost of meeting that load with respect to the capacity factor of the coal facility is the goal of this analysis.

The capacity factor (CF) of generator i is defined as:

$$CF_i = \frac{G_i}{G_{i,capacity}} \tag{B1}$$

where G_i is the output of the generator, and $G_{i,capacity}$ is the nameplate capacity of the generator.

The specific cost of producing one MWh from generator i is defined as:

$$c_i = A_i \cdot CF_i + B_i + C_i \tag{B2}$$

where the A_i, B_i and C_i terms refer to the cost parameters specified in Table 3. The c_i term has units of CAD/MWh. The specific cost for the coal facility is denoted c_c, and is written as:

$$c_c = A_c \cdot CF_c + B_c + C_c \tag{B3}$$

The specific cost for a nuclear facility is denoted c_n, and does not include an A_i or C_i term due to the assumption that the values of these coefficients are zero. c_n is written as:

$$c_n = B_n \tag{B4}$$

The total cost of operating both facilities has the units of CAD and is given by:

$$Cost = c_c \cdot G_{c,capacity} \cdot CF_c + c_n \cdot G_{n,capacity} \cdot CF_n \tag{B5}$$

The sum of the output of each facility must satisfy the given load (demand), which gives Equation (B6).

$$Demand = G_{c,capacity} \cdot CF_c + G_{n,capacity} \cdot CF_n \quad \text{(B6)}$$

Equation (B6) is re-written to solve for $G_{n,capacity} \cdot CF_n$:

$$G_{n,capacity} \cdot CF_n = Demand - G_{c,capacity} \cdot CF_c \quad \text{(B7)}$$

Equation (B7) is then substituted into Equation (B5) to yield:

$$Cost = c_c \cdot G_{c,capacity} \cdot CF_c + c_n \cdot \left(Demand - G_{c,capacity} \cdot CF_c \right) \quad \text{(B8)}$$

Equations (B3) and (B4) are then substituted into Equation (B8) to yield:

$$Cost = \left(A_c \cdot CF_c + B_c + C_c \right) \cdot G_{c,capacity} \cdot CF_c + B_n \cdot \left(Demand - G_{c,capacity} \cdot CF_c \right) \quad \text{(B9)}$$

Equation (B9) is now a total cost equation with respect to CF_c only, with each other value being a constant parameter. The $G_{c,capacity}$ term is factored from Equation (B9) and the equation is re-written as a quadratic function of CF_c and shown in Equation (B10).

$$\frac{Cost}{G_{c,capacity}} = A_c \cdot CF_c^2 + \left(B_c + C_c - B_n \right) \cdot CF_c + \frac{Demand}{G_{c,capacity}} \cdot B_n \quad \text{(B10)}$$

The CF_c term in Equation (B10) is then varied from zero to one and resulting values of $\frac{Cost}{G_{c,capacity}}$ are obtained. It is this plot, $\frac{Cost}{G_{c,capacity}}$ versus CF_c, that is shown in Figure 32.